University of Leoben

Doctoral Thesis

Plasticity at the Micron Scale: A μLaue Study

Christoph Kirchlechner

Leoben, April 2011

April 25^{st}, 2011

This doctoral thesis was typeset by the use of KOMA-Script and LaTeX 2_{ε}.

Erich Schmid Institute of Materials Science
Austrian Academy of Sciences
Departement Materialphysik
Montanuniversität Leoben
Jahnstrasse 12
A-8700 Leoben
http://www.oeaw.ac.at/esi

Affidavit

I declare in lieu of oath, that I wrote this thesis and performed the associated research myself, using only literature cited in this volume.

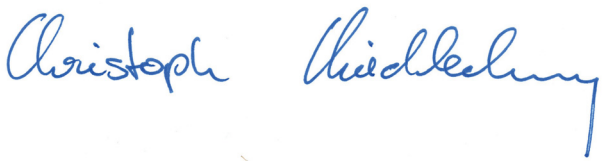

Leoben, April 2011

Acknowledgements

This thesis would not have been possible without the support of a huge number of collaborators, whose engagement I deeply acknowledge.

Foremost, I'm very grateful to my doctoral advisor Prof. Gerhard Dehm, who has supported and guided me all along during this thesis. Furthermore, I want to thank my second supervisor Univ. Doz. Dr. Jozef Keckes.

A synchrotron experiment needs a synchrotron beam. During my thesis Dr. Jean-Sebastien Micha and Dr. Olivier Ulrich provided the ideal machine for the experiments and I'm very grateful for their support and hard work, sometimes during the night. Furthermore I'm very grateful to Prof. Rozaliya Barabash, Prof. Olivier Thomas, Dr. Stephane Labat and Dr. Olivier Perroud for answering my questions on Laue diffraction, XMAS and for measuring some samples.

I warmly thank Gabi Moser, Ing. Herwig Felber and Franz Hubner for preparing samples, for manufacturing numerous small parts and the straining device. Furthermore, I appreciate the support by Doris Schrutt, who did the financial as well as organizational administration enabling me to focus on my work.

Thanks to my good friends and colleagues Marlene Kapp, Wolfgang Grosinger, Dipl. Ing. Peter Imrich and Dr. Christian Motz, who have contributed to this thesis in many ways. Thank you for joining the experiments, thank you for your assistance during data evaluation, for the fruitful discussions, your suggestions and finally for the great working atmosphere. Furthermore, I thank Mag. Sepp Kreith, Dipl. Ing. Matthias Bartosik, Dipl. Ing. Stefan Wurster, Dr. Klaus Jürgen Martinschitz, Dr. Walther Heinz and Dr. Daniel Kiener for sharing the office, literature and some samples.

Obviously the biggest share on this thesis was spent by my parents, which was much more than just physical. Thank you for all possibilities you offered me as well as for the guidance and love you spent during my entire life. Thanks also to my brothers Tobias and Martin for being an incredible family.

Finally, I'm deeply grateful to my beloved wife Ines.

Abstract

The mechanical response of micron and sub-micron sized, single crystalline metallic samples strongly depends on their size. A fact which is neither expected, nor fully understood, but also a fact which has been proven by several studies during the last decade. The reasons for this size dependency are numerous: On the one side there is a clear transition from a collectively controlled to a stochastic dislocation behavior. On the other side the size of a dislocation is naturally restricted by the sample size, which requires higher stresses for dislocation multiplication.

For a thorough understanding of plasticity in small dimensions it is inevitable to observe dislocations *in situ* during plastic deformation, i.e. during multiplication, slip and annihilation. Besides *Transmission Electron Microscopy (TEM)*, which enables the observation of single dislocations, synchrotron based micro-diffraction techniques (as for instance μLaue-diffraction) can provide insights into the collective behavior of dislocations. The aim of this thesis is to contribute to the understanding of size dependent plasticity by μLaue diffraction experiments.

The thesis is devided in three parts: (i) *Post mortem* μLaue diffraction on samples which have been deformed *in situ* in the *Scanning Electron Microscope (SEM)*; (ii) Design of a straining device able to perform *in situ* μLaue experiments on micron sized samples under tension; (iii) *In situ* compression and tensile experiments on micron sized single slip oriented Copper samples during μLaue diffraction.

The results show (i) the unpredicted activation of a slip system at low strains and allow for the estimation of schematic slip mechanism maps; (ii) A device which is able to perform tension, compression and bending, as well as bending fatigue experiments, for samples at the micron scale with an accuracy of approximately 10μN and $1nm$; (iii) Tensile experiments on approximately $6\mu m$ sized samples which show expected and unexpected plastic behavior at the micron scale. Furthermore, the impact of experimental constraints and imperfections on the dislocation structure is shown by *in situ* compression tests.

Kurzfassung

Die Fließgrenze von einkristallinen Metallen unter uniaxialer, monotoner Beanspruchung ist größenabhängig. Ein Faktum welches weder erwartet noch vollständig verstanden ist, aber ebenso durch dutzende Versuche innerhalb des letzten Jahrzehnts bestätigt wurde. Plastische Verformung in diesen Dimensionen wird – so wie im makroskopischen Bereich – durch die Bewegung von Gitterdefekten, sogenannten Versetzungen, ermöglicht. Es ist daher naheliegend, dass das Verhalten von Versetzungen größenabhängig ist und zu einem Wechsel von kontinuierlicher zu stochastischer Verformung mit abnehmender Probengröße führt.

Aus diesem Grund ist es auch unausweichlich, Versetzungen während der plastischen Verformung *in situ* zu beobachten. Dies kann einerseits – im Falle einzelner Versetzungen – durch ein *Transmissions Elektronen Mikroskop (TEM)* geschehen, andererseits kann das kollektive Verhalten von Versetzungen mit Hilfe von μLaue-Diffraktion studiert werden. Ziel dieser Arbeit ist, mit Hilfe von μLaue-Diffraktion zum Verständnis der Plastizität in kleinen Dimensionen beizutragen.

Die Arbeit teilt sich in drei Abschnitte: (i) *Post mortem* Untersuchung von Zugproben die *in situ* in einem Rasterelektronenmikroskops (REM) verformt wurden. (ii) Entwicklung einer Zugapparatur die *in situ* μLaue Experimente an Mikrometer kleinen Proben ermöglicht und (iii) die Durchführung von *in situ* Zug- und Druckversuchen an wenige Mikrometer kleinen, einkristallinen Proben während μLaue-Diffraktion.

Die Ergebnisse zeigen (i) die unerwartete Aktivierung eines Gleitsystems mit niedrigem Schmid-Faktor. Weiters ermöglichen die *ex situ* Experimente die Erstellung schematischer Abgleit-Mechanismen Karten. (ii) Eine Testapparatur, welche Mikrometer kleine Proben *in situ* ziehen, drücken, biegen und ermüden kann wurde entwickelt. Die dabei erreichte Auflösung beträgt ungefähr $10\mu N$ beziehungsweise $1nm$. (iii) Zugversuche an circa $6\mu m$ großen Proben, die einerseits erwartetes, makroskopisches Verhalten, andererseits aber unerwartets Verhalten zeigen, wurden *in situ* am Synchrotron durchgeführt. Schlussendlich zeigen *in situ* Druckversuche den Einfluss von instrumentellen Randbedingungen und Fehlern bei der Versuchsdurchführung auf die Versetzungsstruktur miniaturisierter Proben.

Difficilia quae pulchra
Desiderius Erasmus Roterodamus (1466 – 1536)

Contents

1 Introduction

Plastic deformation sets in at the yield point, the point where a permanent change in shape is caused by an applied stress. From a rather technical point of view the yield point at constant temperatures and strain rates inherently depends on the material, i.e. the chemical composition and the micro-structure, also including the density and type of lattice defects. The validity of this observation has never been doubted. However, the ongoing trend for a miniaturization of devices for *Micro-Electro-Mechanical Systems (MEMS)* and the ability to perform uniaxial compression tests on micron or even sub-micron sized samples revealed an unexpected size effect on the yield stress: Smaller crystalline metals tend to exhibit a significant higher yield stress than their macroscopic counterparts. Uchic and co-workers were the first to report this paradigm in 2004 [1] and still, scientists worldwide are attracted to this phenomenon. The aim of this thesis is to contribute to the understanding of size dependent plasticity by *in situ* μLaue diffraction. For a deeper understanding it is inevitable to learn more about the nature of plasticity, which will be briefly reviewed in chapter 2.

2

Fundamentals of Plastic Flow in FCC Metals

2.1 The Dislocation

Plastic deformation in face centered cubic (FCC) metals at moderate temperatures and strain rates is mainly governed by the movement of dislocations [2, 3]. These are line defects in the crystal caused by the insertion of extra half planes as shown in Fig. 2.1. For a more practical treatment, a dislocation is characterized by two parameters: the line element u and the Burgers vector b. The line element is a unity vector tangential to the dislocation line, the line along imperfections of the crystal can be observed. The definition of the Burgers vector is based on the Burgers circuit [4], a rectangular circuit with an discrete number of steps in horizontal and vertical direction. In a dislocation free crystal the end of the Burgers circuit coincides with the start of it (see Fig. 2.1a). This does not occur if a dislocation is present and an additional vector, the Burgers vector b, is necessary to close the Burgers circuit (Fig. 2.1b)[1]. In fact, this Burgers vector represents the direction and magnitude of the smallest imaginable plastic deformation. It has to be pointed out that the dislocation line can individually proceed through the crystal, whereas the Burgers vector is fixed for a dislocation (see Fig.2.2).

The Burgers vector b can take any angle to the line element u, nevertheless, two important cases have to be mentioned: If the Burgers vector b is perpendicular to the line element u, the dislocation is called an edge dislocation (see Fig. 2.2). Dislocations with vectors b and u being in line (Fig.2.2) are called screw dislocations. Without proof, the general character of a dislocation defined by b and u can always be split in an edge and a screw character.

[1] Different definitions of closing the Burgers circuit are possible (see for instance [5, 6]).

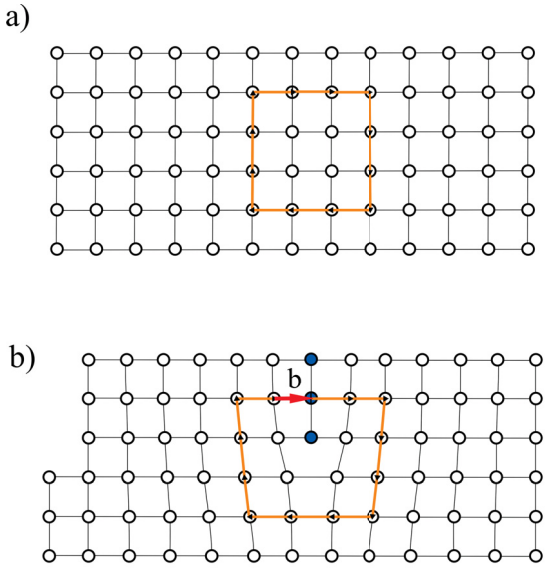

Figure 2.1: Side view on a crystal without (a) and with (b) a dislocation. Additionally the Burgers circuit with the resulting Burgers vector b is shown in (b).

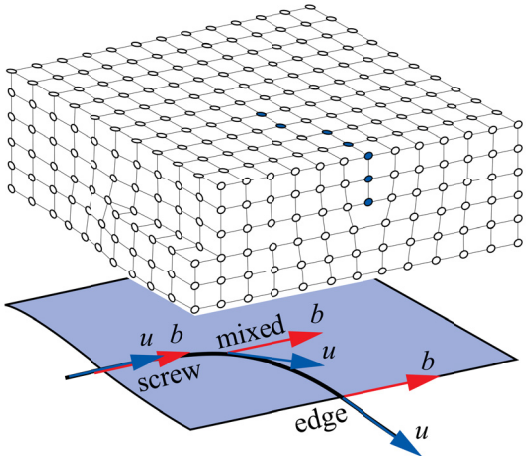

Figure 2.2: Three dimensional sketch showing a crystal penetrated by a dislocation. The projection of the slip plane at the bottom shows that the dislocation line is curved and hence, u changes along the dislocation line, whereas b is fixed. This leads to a screw, a mixed (also called general) and an edge character in one and the same dislocation at different positions.

2.2 Stress Field of a Dislocation

In the vicinity of a dislocation the crystalline lattice is distorted and – according to Hooke's law – stress arises. The stress field of an edge respectively screw dislocation can be described by a tensor as shown in Eq. 2.1 and Eq. 2.2. The magnitude of the single components reciprocally depends on the distance to the dislocation core and further on the Cartesian x and y coordinate. The stress field of an edge dislocation is shown in Fig. 2.3.

It is worth to note that the single components of the stress tensors $\underline{\underline{\sigma}}$ of edge and screw dislocations do not affect each other and, hence, a dislocation including both, screw and edge components, does not split up.

$$\underline{\underline{\sigma}}^{\mathrm{e}} = \begin{pmatrix} \sigma_{xx} & \tau_{xy} & 0 \\ \tau_{xy} & \sigma_{yy} & 0 \\ 0 & 0 & \sigma_{zz} \end{pmatrix} \tag{2.1}$$

$$\underline{\underline{\sigma}}^{\mathrm{s}} = \begin{pmatrix} 0 & 0 & \tau_{xz} \\ 0 & 0 & \tau_{yz} \\ \tau_{xz} & \tau_{yz} & 0 \end{pmatrix} \tag{2.2}$$

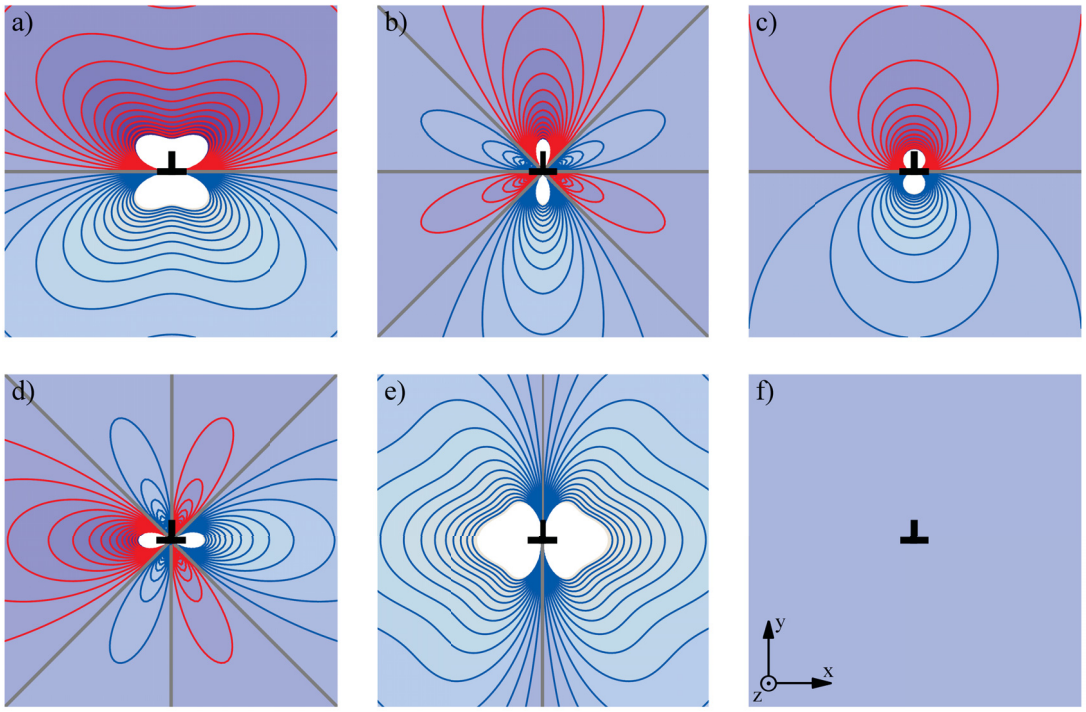

Figure 2.3: Stress field of an edge dislocation with $b = [1\ 0\ 0]$ and $u = [0\ 0\ 1]$. (a) σ_{xx}; (b) σ_{yy}; (c) σ_{zz} for restricted dimensions with sample size equals $10^4 b$; (d) τ_{xy}; (e) van Mises Stress σ_V and (f) σ_{zz} for a crystal with a Poisson's ratio ν equal to zero. Red contours indicate compressive, blue lines tensile stresses.

As a consequence of crystal distortion elastic energy is stored, which can be estimated via Eq. 2.3, where $E^{(\mathrm{u})}$ is the line energy per unit length and G is the shear modulus. Due to the quadratic dependency of the energy, short Burgers vectors are favored. This limits the number of naturally observable Burgers vectors in FCC metals to $b = {}^1/_2\langle 1\ 1\ 0\rangle$ or even split into, for instance $b = {}^a/_2[1\ \bar{1}\ 0] = {}^a/_6[2\ \bar{1}\ \bar{1}] + {}^a/_6[1\ \bar{2}\ 1]$, with a being the lattice constant. For a thorough review on the elastic energy of a dislocation the reader is referred to [7–9].

$$E^{(\mathrm{u})} \approx \frac{G\underline{b}^2}{2} \tag{2.3}$$

Dislocation interaction is based on their stress field. Reducing the stress field generally leads to a decrease of the total elastic energy and hence, mobile dislocations tend to move towards a state of minimal configurational energy. The thereby acting forces on a dislocation i can be described by the Peach-Koehler-Equation 2.4. Note that the origin of the stress field $\underline{\underline{\sigma}}$ in Eq. 2.4 can either be a second dislocation, or simply an externally applied stress.

$$\underline{F} = (\underline{\underline{\sigma}}\,\underline{b}^i) \times \underline{u}^i \tag{2.4}$$

The interaction of two identical dislocations A and B with b in [1 0 0] and u in [0 0 1] is shown as an example. Dislocation A causes a stress field $\underline{\underline{\sigma}}^{\mathrm{A}}$ with components according to Eq. 2.1. The Peach-Koehler-Force F is acting on dislocation B with two non-zero components (Eq. 2.5, Eq. 2.6). One of these components $\tau_{xy}^A b_x^B u_z^B$ acts in a plane spanned by b and u and is called gliding component. The second component acts perpendicular to this plane and is called climbing component. Since the resistance of a FCC metal[2] to dislocation glide is considerably smaller than the resistance to dislocation climb[3], the force component in gliding direction s plays a crucial role for the plastic deformation. The plane spanned by b and u is called slip or glide plane and gliding of edge dislocations will take place here. In contrast, the parallel vectors b and u of a screw dislocations do not form a plane and screw dislocations can cross-slip.

$$\underline{F} = \left(\begin{pmatrix} \sigma_{xx}^A & \tau_{xy}^A & 0 \\ \tau_{xy}^A & \sigma_{yy}^A & 0 \\ 0 & 0 & \sigma_{zz}^A \end{pmatrix} \begin{pmatrix} b_x^B \\ 0 \\ 0 \end{pmatrix} \right) \times \begin{pmatrix} 0 \\ 0 \\ u_z^B \end{pmatrix} \tag{2.5}$$

$$\underline{F} = \begin{pmatrix} \sigma_{xx}^A b^B \\ \tau_{xy}^A b_x^B \\ 0 \end{pmatrix} \times \begin{pmatrix} 0 \\ 0 \\ u_z^B \end{pmatrix} = \begin{pmatrix} \tau_{xy}^A b_x^B u_z^B \\ -\sigma_{xx}^A b_x^B u_z^B \\ 0 \end{pmatrix} \tag{2.6}$$

Fig. 2.4 visualizes the Peach-Koehler-Force caused by dislocation A onto a second dislocation B at position (x, y). It is useful to split $\underline{F}$ into gliding and climbing components. The gliding component attracts each equally signed dislocation in the upper and lower quadrant and repulses identical dislocations in the other two quadrants. As a consequence dislocations form regular patterns: Attracted dislocations are being aligned one below the other and form a tilt sub-grain boundary.

2.3 Schmid's Law

A mobile dislocation will move on its glide plane due to the Peach-Koehler-Force given in Eq. 2.4 when a critical limit is exceeded. This limit inherently depends on the material[4] as well as on the crystallographic plane and is called the critical shear

[2] at moderate temperatures

[3] Climbing requires a sufficient degree of diffusion and is therefore limited to a temperature of $T \geq 0.5 T_m$, with T_m being the melting temperature.

[4] in case of body centered cubic (BCC) crystals it depends also strongly on the temperature

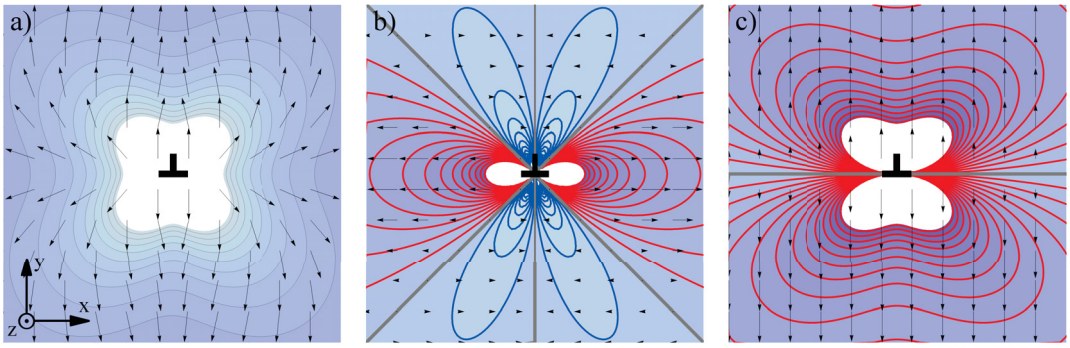

Figure 2.4: Peach-Koehler-Force caused by the stress field of dislocation A in the center is acting on dislocation B at position (x, y). (a) Vector field and magnitude of $\underline{F}$; (b) direction and magnitude of the gliding component; (c) direction and magnitude of the climbing component. Red contours indicate repulsive forces, blue contours denote attraction.

stress τ_c. The crystallographic plane with the lowest possible critical shear stress (Peierls stress) is generally the closest packed plane, which is (1 1 1) in case of FCC metals. This is essentially the main finding of Erich Schmid[5] and co-workers [10].

Assume an uniaxially stressed rod: The shear stress acting on one slip plane depends, according to Fig. 2.5, on the angle between the tensile axis Z and the slip plane normal vector n, as well as on the angle in between Z and the gliding direction. The slip (or gliding) direction s is hereby always along b. This leads to the better known formulation of Schmid's law (2.7-2.9):

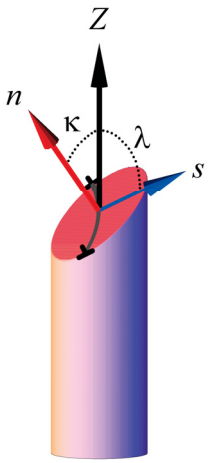

Figure 2.5: Uniaxially stressed rod: Z direction of applied force; n slip plane normal vector; s slip direction (corresponds to b); λ angle in between Z and s; κ angle in between Z and n.

$$\tau = \frac{F}{A} \cos\kappa \cos\lambda \geq \tau_c \tag{2.7}$$

[5] In honor of this early work the Austrian Academy of Sciences named its institute for Material Science after Erich Schmid.

$$\tau = \frac{F}{A}\frac{\underline{n}.\underline{Z}}{|\underline{n}||\underline{Z}|}\frac{\underline{s}.\underline{Z}}{|\underline{s}||\underline{Z}|} \geq \tau_c \tag{2.8}$$

$$\tau = \frac{F}{A}m = \sigma m \geq \tau_c \tag{2.9}$$

Whereas m is the Schmid factor which is ranging from $0.0 - 0.5$, A represents the cross-sectional area and F equals the applied force. Consequences of Schmid's law onto the deformation behavior of uniaxially loaded samples will be discussed in the next section.

For a general stress state the entire Schmid tensor needs to be calculated, which is given by the dyadic product of the slip direction $s^{(\alpha)}$ and the slip plane normal $n^{(\alpha)}$ for each slip system (α) according to Eq. 2.10. The resolved shear stress $\tau^{(\alpha)}$ can then be calculated (2.11):

$$\underline{\underline{P}}^{(\alpha)} = \frac{1}{2}\left(\underline{s}^{(\alpha)} \otimes \underline{n}^{(\alpha)} + \underline{n}^{(\alpha)} \otimes \underline{s}^{(\alpha)}\right) \tag{2.10}$$

$$\underline{\underline{\tau}}^{(\alpha)} = \underline{\underline{\sigma}}.\underline{\underline{P}}^{(\alpha)} \tag{2.11}$$

2.4 Single and Multiple Slip

The findings of the previous section allow for a deeper discussion of single crystal plasticity under uniaxial load. Twelve $\{1\ 1\ 1\}\langle 1\ 1\ 0\rangle$ slip systems are available in a FCC lattice [11]. Depending on the orientation of the straining axis in the crystal coordinate system, the slip system exhibiting the highest resolved shear stress (and therefore also the highest Schmid factor) will be activated. The magnitude of the highest available Schmid factor is shown in the positive hemisphere of the orientation space in Fig. 2.6a.

The highly symmetric pattern in Fig. 2.6a is caused by the crystal symmetry of the FCC lattice and allows for a generalization of orientation dependencies of the Schmid factor by a projection into a unit triangle, a spherical triangle with corner-points at the [0 0 1], [0 1 1] and the [1 1 1] pole. Note that in a unit triangle – also called inverse pole figure [12] – the crystal coordinate system is fixed and the straining axis is plotted as a certain direction. The Schmid factor of the primary slip system $m^{(1)}$ – the system exhibiting the highest Schmid factor – is shown in the unit triangle presented in Fig. 2.7a. In maximum the Schmid factor is 0.5, appearing at a straining axis of approximately $\langle 9\ 2\ 20\rangle$. In minimum $m^{(1)}$ is 0.27 if the straining axis coincides with the $\langle 1\ 1\ 1\rangle$ axis in this case. Therefore, the $\langle 1\ 1\ 1\rangle$ axis is called "hard direction".

The unit triangle representing the second highest available Schmid factor $m^{(2)}$ is shown in Fig. 2.7b. Here, the actual slip-system exhibiting $m^{(2)}$ changes within the plot. Depending on the position in the unit triangle, three different slip systems can attain $m^{(2)}$ making the unit triangle inappropriate to use for $m^{(2)}$. More important is Fig. 2.7c, showing the difference in Schmid factor of the primary compared to the secondary slip system according to Eq. 2.12.

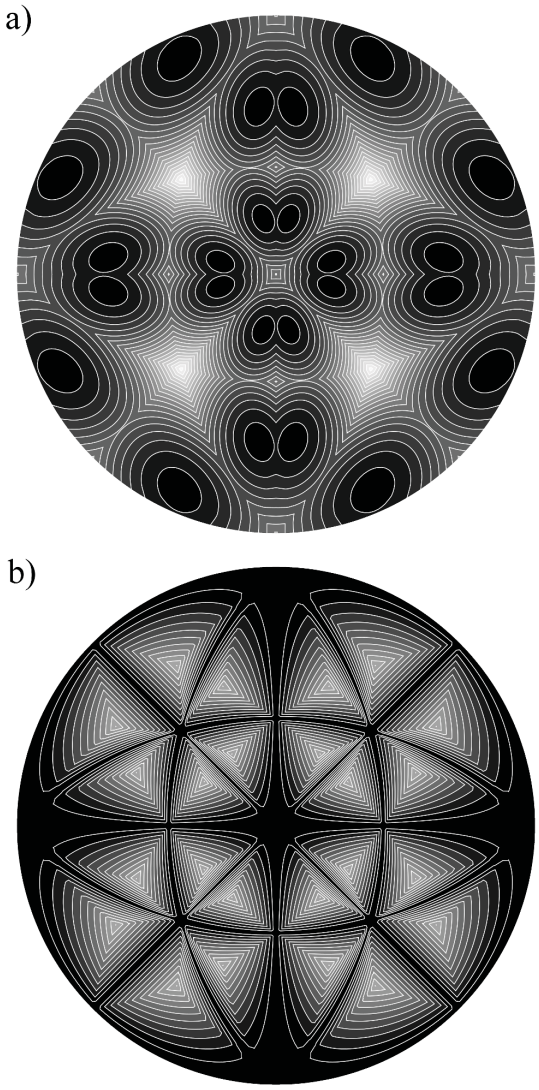

Figure 2.6: (a) The magnitude of highest available Schmid factor is plotted in the positive hemisphere of the orientation space. Dark contours indicate a high Schmid factor. (b) Difference of the highest and the second highest available Schmid factor according to Eq. 2.12. Black regions indicate multiple slip.

$$\Delta m^{(1-2)} = \frac{m^{(1)} - m^{(2)}}{m^{(1)}} \tag{2.12}$$

Inside the unit triangle a non-zero difference $\Delta m^{(1-2)}$ exists, favoring dislocation slip on just one slip system. These are single slip orientations, whereas the ideal single slip orientation with $\Delta m^{(1-2)} = 27.5\%$ is not a simple crystallographic axis and approximately equals the $\langle 5\,3\,8 \rangle$ axis. In contrast, the difference $\Delta m^{(1-2)}$ equals zero at the borderlines of the unit triangle and therefore, at least two equally favored slip systems exist and multiple slip will take place. In fact, the number of coexisting slip systems with the same Schmid factor equals the number of adjacent unit triangles. A good overview on single and multiple slip orientations is given in Fig. 2.6b.

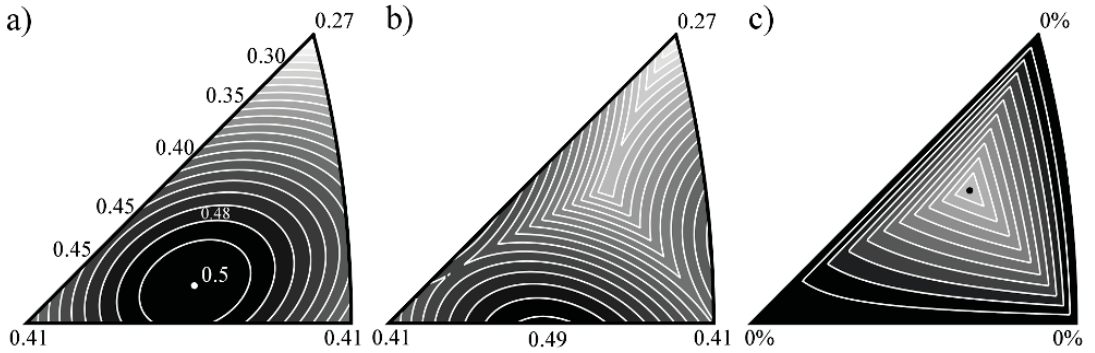

Figure 2.7: Standard triangles representing (a) the highest available Schmid factor $m^{(1)}$; (b) the second highest Schmid factor $m^{(2)}$ and (c) the difference between the highest and the second highest Schmid factor $m^{(1-2)}$.

These fundamental findings however require (i) an uniaxial stress state (ii) a slip plane independent τ_c and (iii) the availability of mobile dislocations. (i) is influenced by experimental constraints and imperfections. (ii) is most likely to be fulfilled, except the dislocation population acting as friction force is not randomly distributed over all slip systems of the crystal. (iii) strongly depends on the dislocation population, especially when small dimensions are reached. Hence, the downscaling of this concept will be part of the experiments presented in this work.

2.5 Dislocation Multiplication

So far the movement of a mobile dislocation has been discussed, assuming that a sufficient number of mobile dislocations is stored in the deformed volume. Experiences show that this assumption is simplifying and only applicable with a limited scope. As a second key mechanism dislocations need to multiply during plastic deformation. The multiplication of a dislocation takes place at a dislocation source. This can either be a nucleation site at the surface or a source dislocation, such as the later discussed Frank-Read-Source [13].

The multiplication of a dislocation at the sample surface is scarce in case of metals, since other sources require much less stress to multiply [14]. It is assumed that such a heterogeneous multiplication only takes place if no other dislocation sources were present. However, the multiplication at the sample surface is self-explanatory (see Fig. 2.2).

Much more important is the multiplication within a Frank-Read-Source (FRS) as shown in Fig. 2.8. A mobile dislocation is pinned at two points. A force F proportional to the applied stress τ acts on the dislocation according to Eq. 2.4 and the dislocation will bow out in between the two fixed points. The line tension of the dislocation counteracts the bow out and tries to reduce the length of the dislocation segment. At a radius $r = 1/2L$ an instable configuration is reached: The applied force equals the line tension $\propto 2Gb^2$. Any further increase of τ leads to a spontaneous increase of the dislocation length, as long as the two segments forming a spiral around the pinning

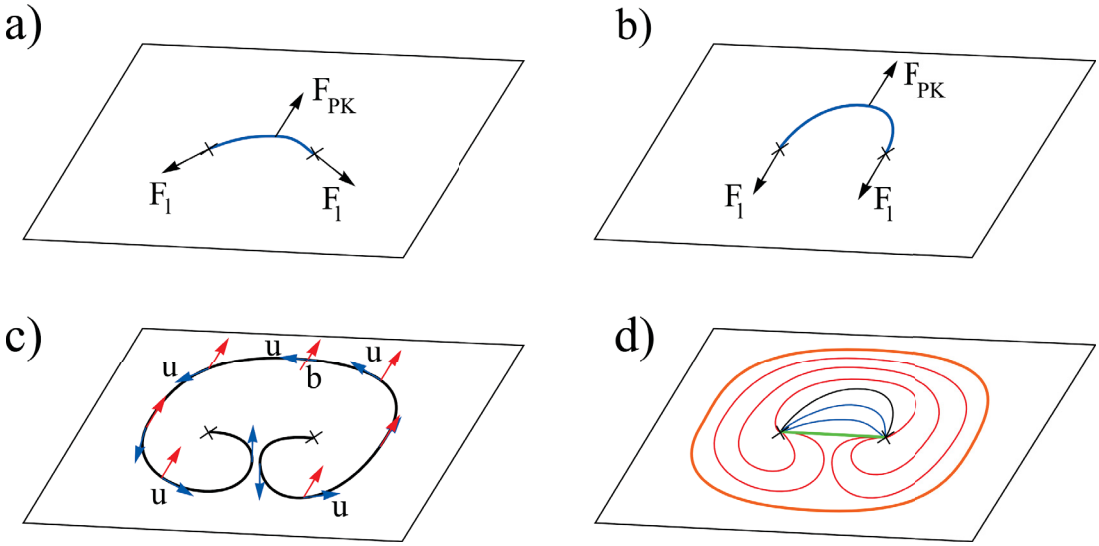

Figure 2.8: Frank-Read-Source: (a) stable bow-out with acting Peach-Koehler-Force and line tension; (b) an instable state is reached when the line tension is in opposition to the acting Peach-Koehler-Force; (c) annihilation due to the opposite dislocation character; (d) all stages during the multiplication, including the initial and the produced dislocation.

points meet. Due to their opposite character the dislocation annihilates (see next section): The old dislocation source is being rebuilt and the new, circular dislocation is expanding. As long as the new dislocation is able to freely move away it will not affect the dislocation source, which can restart again. If the new dislocation is not able to move away a stress (called a back-stress) in opposition to the applied shear stress τ arises which might shut down the dislocation source. The maximum required stress during the multiplication process appears at the point of the instable dislocation configuration. A simple force equilibrium can be used to estimate this shear stress; L equals the distance of the two pinning points (see Eq. 2.13).

$$\tau^{FRS} = \frac{2Gb}{L} \tag{2.13}$$

Essential for the operation of the FRS is the fixation of the dislocation line at the two fixing points (see Fig.2.8), which can either be a second dislocation or any other obstacle. A variation of the FRS is the Koehler source with pinning points developed during the cross slip of an initially straight screw dislocation. This is believed to be the dominant multiplication mechanism in crystals with low dislocation density, for instance in LiF [15]. A thorough discussion on dislocation based pinning points is given by Nix and co-workers in [16].

2.6 Dislocation Annihilation

Dislocations of opposite sign attract each other due to the Peach-Koehler-Force and – if they are situated on the same slip plane – annihilate. This direct annihilation is serendipity. But in fact, even if the dislocations are not situated on the same slip plane,

they attract each other, align one below another and form an immobile arrangement[6].

A much easier and more likely way for dislocation annihilation is simply the escape to the sample surface. This process routinely takes place in crystals of each size and is evidenced by the formation of slip steps on the surface. This can be used to identify the activated slip plane. In Fig.2.9 an example of micron sized samples exhibiting single and multiple slip is presented, where dislocations of one respectively two different slip systems escaped to the sample surface.

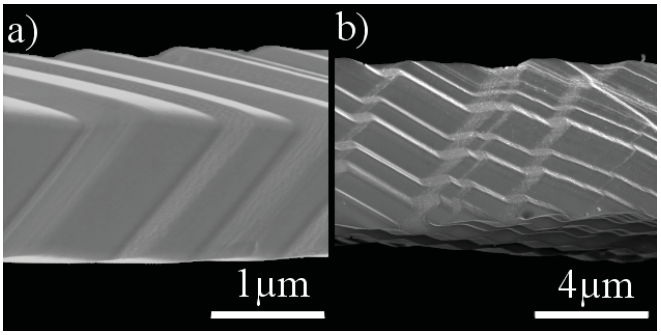

Figure 2.9: *Scanning Electron Microscopy (SEM)* image of single crystalline copper samples exhibiting (a) single and (b) multiple slip.

This process does not necessarily need an externally applied stress: All stress components perpendicular to the surface must vanish at the surface and, though, cause an asymmetric stress field which pushes the dislocation to the surface. The thereby acting force can – at least in case of screw dislocations – be easily estimated. Assume two screw dislocations A and B, whereas the magnitude of the Burgers vector of dislocation A is $|\underline{b}^A|$ which equals $|\underline{b}^B|$, with $\underline{b}^A$ and $\underline{b}^B$ having opposite directions. Dislocation A is situated inside of the material with a distance d to the surface. Dislocation B is a virtual dislocation situated outside of the material, again with a distance d to the surface, which means that the surface is exactly in between the two screw dislocations. The Peach-Koehler-Force acting on dislocation A caused by the virtual dislocation B leads to an attracting component towards the surface and furthermore to a vanishing component in the surface. This special force is called the *Image Force* [17] of a dislocation. A fundamental consequence of the image force is, that mobile dislocations close to the sample surface automatically escape at the surface, which might lead to a dislocation free crystal in nanometer length scale dimensions.

[6] In this case only the Peach-Koehler-Force in gliding direction vanishes. Provided that the temperature is sufficiently high for diffusion, the dislocation cores will converge due to the climbing component and annihilate with time.

3

Size Dependent Single Crystal Plasticity

3.1 Size Dependent Strengthening Effects

Size dependent plasticity attracted scientists since plastic deformation has been explained by the collective movement of dislocations. A prominent example for this is the Hall-Petch [18, 19] relation interlinking the grain size with the increase in flow stress σ_y according to Eq. 3.1, where σ_0 is the friction stress for materials without grain-boundaries, K is the grain boundary resistance and d is the average grain diameter.

$$\sigma_y = \sigma_0 + \frac{K}{\sqrt{d}} \tag{3.1}$$

The concept of Hall and Petch is based on the internal barrier imposed by grain-boundaries. To break through a grain boundary a certain stress has to act on the dislocation, leading to a pile-up. The density and structure of the grain boundary determines the resistance to dislocation motion and the mechanical response of the material. The density of grain-boundaries enters Eq. 3.1 with the average grain diameter, which is an internal length scale. Similar size effects based on internal length scales are given by Arzt in [20]. Size effects based on an internal length scale are not within the focus of this work and will not be discussed here.

Non-uniform deformation can also cause an increase of flow stress due to the storage of *Geometrically Necessary Dislocations (GNDs)* as defined in Eq. 3.2, with ρ_{GND} equalling the density of GNDs, γ being the shear on a slip system and x pointing in the direction of the gradient.

$$\rho_{GND} = \frac{1}{b}\frac{\partial \gamma}{\partial x} \tag{3.2}$$

The GNDs thereby have to accommodate non-uniform deformation and are proportional to a strain gradient $\partial\gamma/\partial x$. The GNDs are necessary to keep the integrity of an non-uniformly deformed crystal[1]. The GNDs affect the strength of the material similar to *Statistical Stored Dislocations (SSDs)* which can be described by a Taylor equation (Eq. 3.3). Here, τ_y is the shear yield strength and α is a numerical constant in the range of $1/2$.

$$\tau_y = \alpha G b \sqrt{\rho_{SSD} + \rho_{GND}} \tag{3.3}$$

As written in Eq. 3.3, the size dependency of the flow-stress is not obvious. However, strain gradient plasticity models can be used to explain the thickness effects as described by Fleck et al. [21] and Stölken and Evans [22]. Another interesting size effect, called *Indentation Size Effect (ISE)* [23] which occurs during nano-indentation, can partly be explained by strain gradient plasticity [24]. However, size effects based on strain gradients are not within the focus of this work, but might result in a contribution to size dependent flow-stress phenomenons due to experimental imperfections.

Today, there is a global understanding of size effects caused by internal length scales – as manifested in different models which describe the influence of defects on the strength of materials. This led to the knowledge that not only the chemical composition but rather the defect densities, and hence the internal length scales, influence the strength of a material.

3.2 Size Effects Under Uniaxial Loading

If all internal barriers[2] are excluded and an uniaxial test is being performed ideally, the yield point tends to increase significantly when the sample size is being reduced [1]. This is not expected, since single crystal plasticity theories do not include any size dependencies. However, several studies followed the pioneering work of Uchic and proofed the "smaller is stronger" paradigm for different FCC [1,25–30] and BCC [31–35] metals. This forced material scientists to reconsider the classical theories of plasticity.

The sample size dependency is characterized by different features [36–38]. As mentioned above, the yield point increases with smaller sample diameters. Furthermore, the yield point measured for different, equally sized samples scatters a lot. The stress-strain response exhibits a different behavior compared to macroscopic dimensions manifested by a serrated flow and the observed hardening rates differ from macroscopic values.

3.3 The Current Interpretation of Plasticity in Small Dimensions

Similar to macroscopic dimensions plasticity at the micron and sub-micron scale is governed by dislocations. This is proofed by the formation of distinct slip steps [1, 30]

[1] Other possibilities are cracks or twins.
[2] Except dislocations, which are indeed also responsible for an internal length scale.

and also shown in Fig. 2.9. Furthermore, dislocation free single crystals – so called whiskers – do not show any size dependency as experimentally proofed by Brenner [39] and Bei [40, 41].

In macroscopic dimensions plasticity was triggered by the movement of dislocations. However, at the micron scale the number and size of dislocation sources is limited. This leads to a transition from a movement controlled to a multiplication controlled regime [42]. In fact, the size of a dislocation source is limited by the half sample diameter, which leads to a size dependency of the flow stress according to Eq. 2.13. Here, the flow strength would scale with a power law according to Eq. 3.4 with d being the sample diameter and m being the power law exponent. In case of a purely source size controlled regime the power law exponent m equals -1. This has not been experimentally observed yet. However, the sample dimensions naturally introduce a source size cut off. The differences in m document that this *Dislocation Source Size Truncation* is not the only influence.

$$\sigma_y \propto d^m \tag{3.4}$$

In macroscopic dimensions the number of dislocations – and also the dislocation line length – is very high. Assuming a well annealed single crystal with a size of one centimeter cubed. The dislocation density is in the order of $10^{12}m^{-2}$. This leads to a dislocation line length of 10^6m. If we now take just one cube micron sized sample, which is exactly the dimension we are talking about, the length of dislocations present in the crystal reduces to $10^{-6}m$, which is exactly one dislocation penetrating through the micron sized sample. Obviously, the collective behavior of the dislocations in macroscopic dimensions has to become stochastic at the micron scale and the assumption, that a sufficient number of dislocations is able to multiply is not automatically fulfilled. The dislocations do not have to "sit" on the primary slip system, which might lead to the activation of lower ranked slip systems [43]. Furthermore, in the deep sub-micron regime, a high probability exists that no dislocation is present at all, which then would lead to the observation of the theoretical strength τ_{th}. Generally, such a state will be reached when the dislocation multiplication is slower than the dislocation escape at the sample surface. This behavior has been proposed by W.D. Nix and co-workers in [29, 44] and is called *Dislocation Starvation*.

In a fully dislocation starved specimen the theoretical stress should be observable, except dislocation nucleation as described by Nix and Lee [14] takes place at the sample surface. This is probably promoted by the imperfect surface, but anyhow, should only happen in the deep nanometer regime and is therefore not within the focus of this work.

Both concepts presented, i.e. dislocation starvation [44] and dislocation source truncation [42], are expected to be responsible for the observed size effect. Today, there is still an ongoing discussion on the validity and the size regime of these models, which is mainly caused by the fact that experimental observations do not fully validate any of these concepts. This might be caused by several additional influences which will be thoroughly discussed in the next section.

3.4 Influences on Quantitatively Measured Size Dependent Strengthening Effects

In Fig. 3.1 influences on the size dependency of single crystals proofed by the literature presented in Tab. 3.1 is schematically presented. Both presented models, i.e. dislocation starvation and dislocation source truncation, are based on a specific distribution of dislocations and dislocation lengths, which is of course depending on time and strain. Major influences on the dislocation density are the number and the stability of pinning points, which are themselves partly controlled by the stacking fault energy. This are, in principle, material dependent influences, which should be described by any appropriate model. Unfortunately, real samples show imperfections such as initial strain gradients [45, 46], grain boundaries [45] and surface defects like a focused ion beam (FIB) damage layer [47] or a native oxide layer. These sample imperfections strongly alter the evolution of the dislocation density, the stability of pinning points and result in a different number of mobile dislocations. The evolution of mobile dislocations with time will determine the stress-strain behavior of the sample.

Further influences on the stress-strain behavior are caused by the test conditions, namely if the experiment is performed in real displacement controlled mode (such as done in [30, 48]) or in force controlled mode [1, 26], if there are any vibrations of the setup and if the sample is not properly aligned [49]. In addition, the aspect ratio alters the free volume which allows dislocations to move and, hence, strongly influences the hardening behavior [49–51]. Similar effects are caused by a lateral stiff testing setup which hinders the lateral movement of the sample with respect to the flat punch top and causes an additional stress component, also resulting in hardening. In summary, a lot of imperfections coming from the real sample and the experiment itself blur the stress-strain response of one single sample.

Unfortunately, the above described influences on the stress-strain response have to be extended when a "yield point vs. sample-size" plot is made. It is inevitable to question the definition of the yield point in a general manner, which is indeed much more than answering only a philosophical question. (Plastic) flow leads to an enduring change in the shape of the material. A simple bow out of a dislocation – as presented in Fig. 2.8a – is (almost) reversible if the metastable configuration presented in Fig. 2.8b is not exceeded. Hence, to overcome the elastic (or pseudo-elastic) limit, the dislocation needs to multiply. The elastic limit is well below the resolution of typical instruments used in micro-compression and micro-tension experiments and would further only be noticed when unloading cycles are included[3]. To overcome this problem a technical yield point is defined, which is macroscopically taken at 0.2% plastic strain. Unfortunately, the strain where the yield stress is taken is not standardized and strongly varies (0.2%, 0.5%, 1.0%, 5.0%, 10%, or even 15%). This is clearly above the elastic limit and leads to an intermixing of different aspects of size dependent plasticity, namely the size dependency of the yield point and size dependent hardening effects.

[3] The experiments by Dunstan and Bushby are able to measure the elastic limit on long wires under torsion as shown in [52].

Furthermore, it has to be taken into account that the strength of a material at the micron scale is a statistical property which requires a sufficient number of samples to determine not only the mean values of strength, but also the upper and the lower bound. Unfortunately the mean value does neither describe the lower bound model (dislocation source truncation) nor the upper bound model (dislocation starvation).

Hence, influences caused by real (imperfect) samples, due to test conditions and by data evaluation vary the size dependent response of the material, which prevents a quantification of both models.

3.5 Open Questions

The previously described models, namely dislocation starvation[4] and dislocation source truncation need to be validated. Hereby it is necessary to go beyond measuring solely the stress strain response of a material. It is inevitable to interlink the mechanical behavior to the underlying micro-structure. Methods allowing for this are *Transmission Electron Microscopy (TEM)* [54, 61, 68] and X-ray μLaue diffraction [48, 69, 70]. In the near future, also coherent X-ray diffraction [71–73] may be able to interlink the mechanical behavior with the corresponding dislocation structure. But even when the models are validated and interlinked to different initial dislocation structures fundamental questions in (size dependent) plasticity remain.

The effect of the stacking fault energy onto the dislocation mobility is still not fully understood. This effect is based on the possible split up of a dislocation into partial-dislocations which are unable to cross-slip [74]. Also, the stability of pinning points strongly depends on the stacking fault energy [16], but experimental work is lacking.

One further question is also to identify dislocation interactions during strain hardening. Unfortunately – as pointed out in the last section – hardening is often caused by experimental constraints and imperfections, which obscures the material behavior. It seems to be more advisable to study hardening phenomenons on intrinsic constraints, such as grain or twin boundaries. If the intrinsic constraints surpass the instrumental ones reproducible, inherently material dependent hardening will be observed. The above described *in situ* methods are required to go beyond a continuum mechanical description – which is well known [18, 19] – and describe the discrete interaction of dislocations with obstacles.

[4] Currently there is no mechanism based formalism which can be quantified.

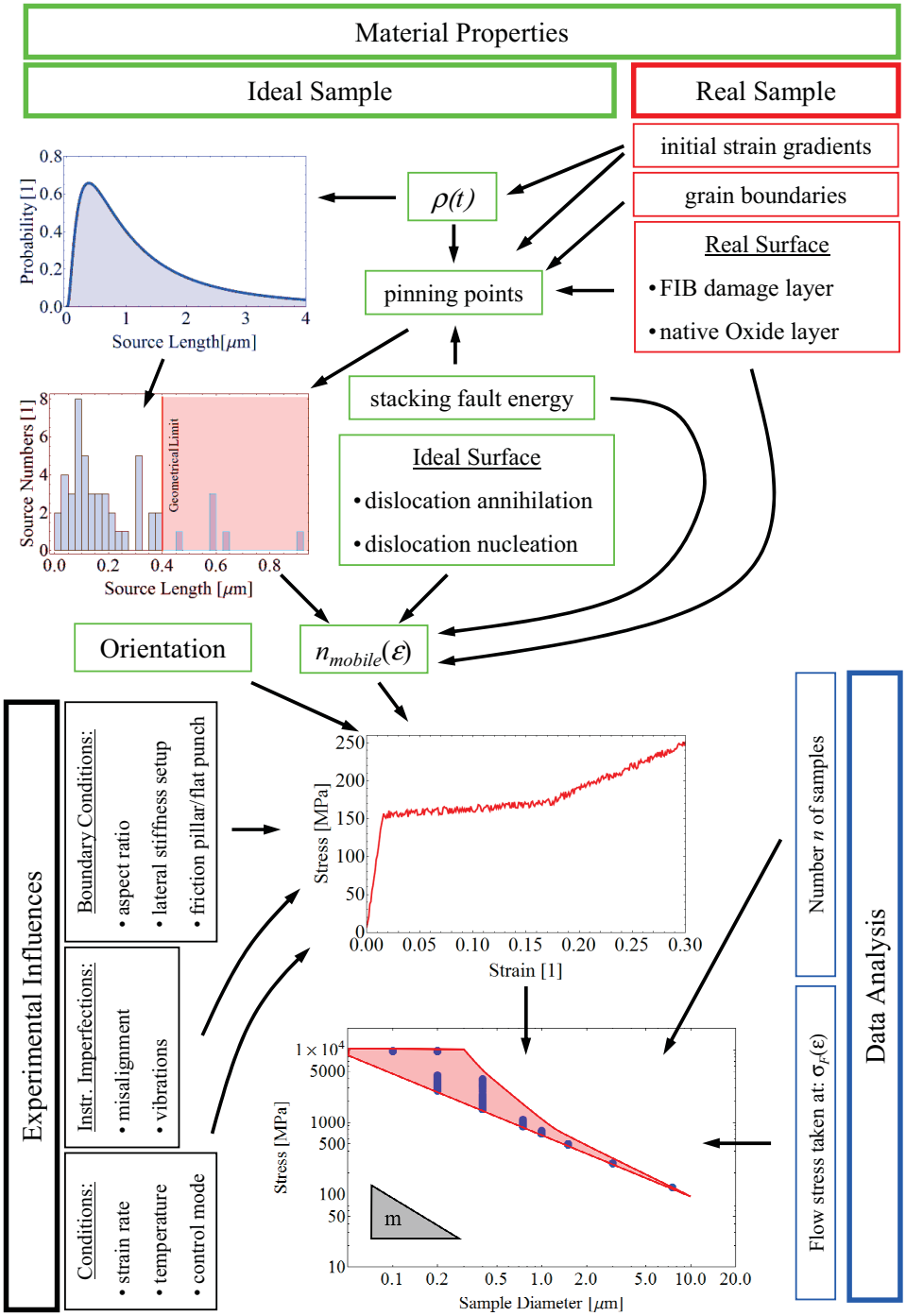

Figure 3.1: Influence of material properties, instrumental constraints and imperfections as well as data analysis on the measured size dependency.

Table 3.1: Literature focusing on different aspects of the sample size effect.

Influence	Experiment	Simulation
Dislocation Density	S.S. Brenner [39]	
	H. Bei et al. [40]	
	H. Bei et al. [41]	
	D.M. Norfleet et al. [53]	
	S.H. Oh et al. [54]	
	R. Maaß et al. [55]	
		H. Tang et al. [56]
		H. Tang et al. [57]
		C. Motz et al. [58]
		J. Senger et al. [51]
Pinning Points	S.W. Lee et al. [16]	
Surface Nucleation	W.D. Nix et al. [14]	
Strain Gradients	J. Zimmermann et al. [59]	
	R. Maaß et al. [45]	
	R. Maaß et al. [46]	
	C. Motz et al. [60]	
FIB-damage	D. Kiener et al. [47]	
	Z.W. Shan et al. [61]	
	H. Bei et al. [41]	
Native Oxide	C.A. Volkert et al. [26]	
	J.R. Greer et al. [27]	
	J.R. Greer et al. [62]	
Instr. Imperfections	H. Zhang et al. [63]	
	Y.S. Choi et al. [64]	
	C. Kirchlechner et al. [49]	
		J. Senger et al. [65]
Boundary Conditions	D. Kiener et al. [66]	
	D. Kiener et al. [50]	
	C. Kirchlechner et al. [49]	
		J. Senger et al. [51]
		F. Roters et al. [67]

4

μLaue Diffraction: a Tool to Probe Imperfect Crystals

4.1 Laue Diffraction

Laue diffraction is the oldest X-ray diffraction method [75] and has been suggested by Max von Laue in order to answer two fundamental questions in modern physics: (i) What is the nature of X-rays and (ii) does a crystal really consist of periodically arranged atoms. Max von Laue was therefore awarded with the Nobel Prize for Physics in 1914. Since then, Laue diffraction has been widely used in Material Science to analyze single crystalline materials.

The sphere of reflection, today known as *Ewald Sphere* [76], allows for the prediction of constructive interference at different lattice planes. If a reciprocal lattice point intersects the Ewald sphere, constructive interference will be observed. In the monochromatic case (powder diffraction, Fig. 4.1a) the Ewald Sphere is very thin and the reciprocal lattice points do not necessarily intersect the sphere. However, by rotating the sample (performing a rocking scan), the reciprocal lattice can be rotated with respect to the incident beam k_0 and at a certain crystal orientation (see Fig. 4.1a) constructive interference will be observed. This time-consuming process leads to additional problems at the micron scale, which will be discussed later. In contrast Laue diffraction uses a broad energy band pass[1]. Thus, the Ewald sphere extends to a finite volume with radii ranging from k_{0max} to k_{0min} (see Fig. 4.1b). Several reciprocal lattice points are lying within this volume and all of those will lead to constructive interference as long as their structure factor is not zero[2].

[1] Also called *White X-ray beam.*

[2] In case of FCC crystals the structure factor is unequal zero if h, k, l are all even or all odd, but equals zero if h, k, l is mixed [77].

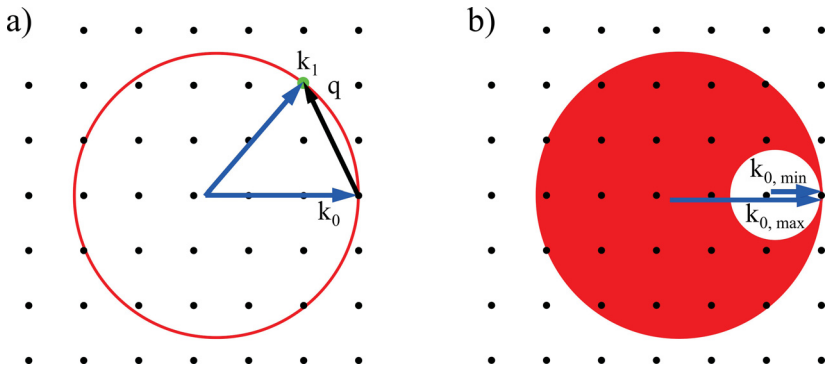

Figure 4.1: Schematic Ewald Sphere (a) of a monochromatic and (b) of a Laue experiment.

A fundamental consequence is, that no sample rotation is required to cause constructive interference, which allows for very fast measurements. Furthermore, all illuminated crystals will automatically contribute to the pattern. This is of major interest in the case of single crystalline, micro-mechanical samples [78] since all sub-grains or even all unexpected, but nevertheless, also present grains will definitely be noticed [45].

However, using a white X-ray beam has a major drawback: The energy of a Laue spot is unknown and, hence, the Laue pattern can not be used to calculate the lattice spacing. This leads to a superposition of Laue spots which stem from parallel lattice planes.

How to Index a Laue Pattern

Fig. 4.2a shows a Laue pattern recorded with an energy ranging from 5-25keV ($\lambda \approx 0.05 - 0.25nm$) on a copper single crystal. Analyzing the Laue pattern can be divided in the following steps:

- background subtraction
- choose a set of n Laue spots (see Fig. 4.2b) and measure the angles α_{ij} between the reflections (Fig. 4.2c). Typically n is ranging from 4-7 [79].
- calculate angles between all possible Laue spots. The number of observable spots is hereby limited by the structure factor and the used energy range.
- compare measured and calculated angles and find the combination with the lowest error
- check whether Laue spots that are not included in the starting set also match the solution

In the underlying work indexing was performed by the software package *X-ray Microdiffraction Analysis Software (XMAS)* [81]. The informations obtained from an indexed pattern are manifold: (i) all Laue spots can be assigned to a lattice plane[3], as

[3]Note that there is an superposition of parallel Laue spots, for instance (1 1 1),(2 2 2)...

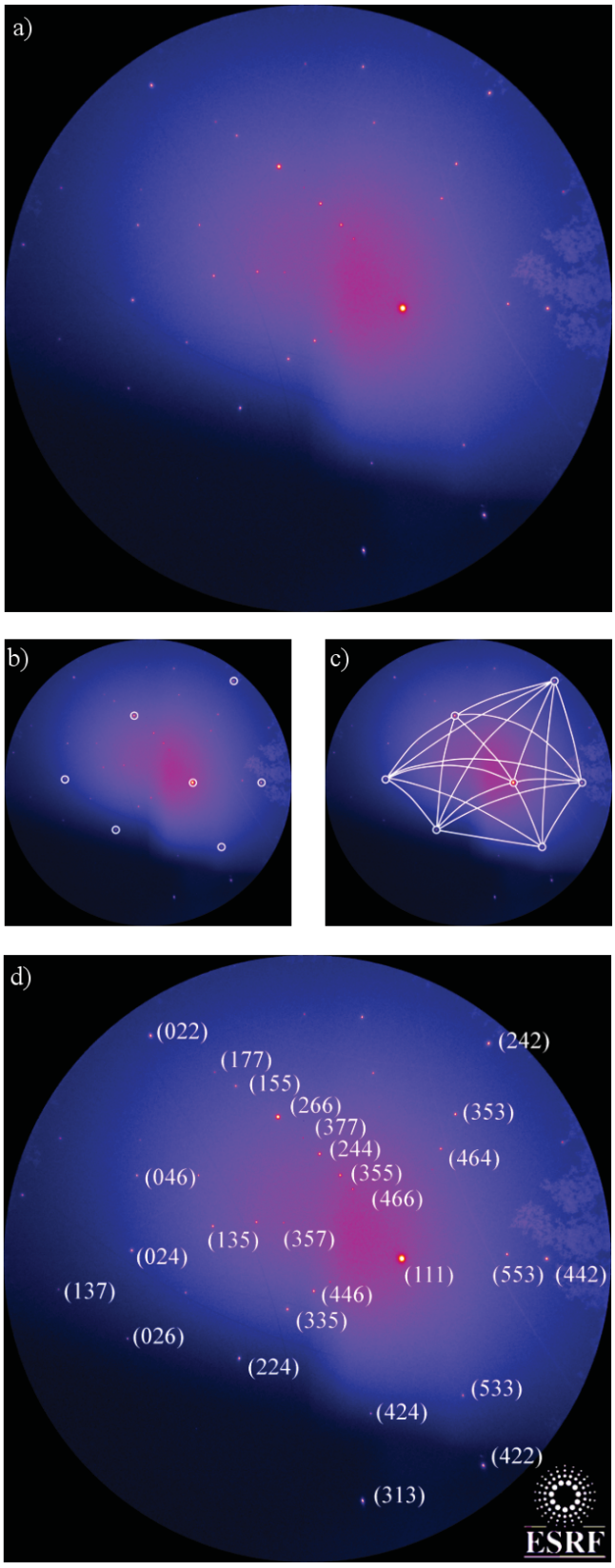

Figure 4.2: (a) Measured Laue pattern; (b) Set of taken Laue spots; (c) Measured angles α_{ij} between the spots; (d) Indexed Laue pattern. The pattern has been measured at the French Beamline CRG-IF (BM32) [80] of the European Synchrotron Source (ESRF), the background is not subtracted.

for instance shown in Fig. 4.2d. (ii) A rotation matrix *CtoS* transforming the crystal coordinate system into the sample coordinate system. (iii) By analyzing the difference off the measured peak position to the ideal position the deviatoric strain tensor[4] could be derived from the Laue pattern. To analyze also the hydrostatic part it is necessary to determine the lattice spacing of selected reflections, which can be done by inserting a tunable monochromator into the primary beam. However, this requires a well calibrated setup.

Limitations of Classical Laue Diffraction and the Need for Small Beam Sizes

The above described procedure cannot be applied in cases where more than approximately 10 grains contribute to the Laue pattern [81]. This is simply based on the fact, that the starting set of spots has to increase (at least four spots per grain) which is very time-consuming. It is not only a question of computing time, but also a way to allocate a spot to a specific grain has to be found, which turns out to become almost impossible if a critical number of grains is present. For instance, in case of copper, being a FCC structure which shows a low number of reflections, at least 30 Laue spots are observed in a typical Laue diffraction setup[5]. If 10 grains are being assumed in the illuminated volume, the number of observed Laue spots increases to approximately 300, which also leads to overlapping spots as presented in Fig. 4.3c-d. Hence, the use of Laue diffraction is limited to problems where the grain size is in the range of the primary beam size (see Ref. [83] and Fig. 4.3a-b).

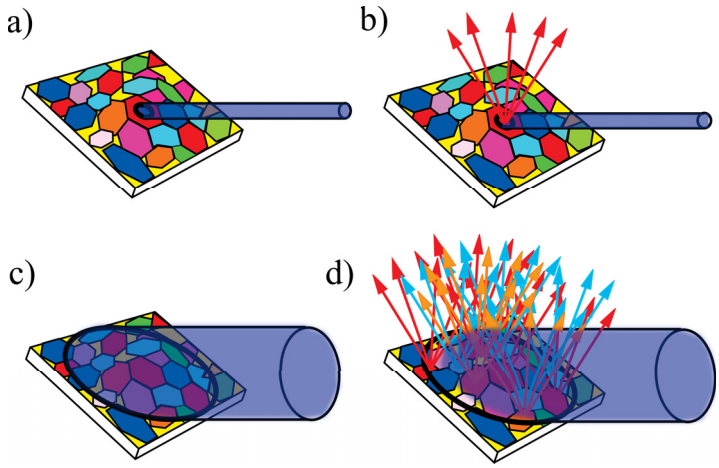

Figure 4.3: (a,b) Primary beam size in the range of the grain size; (c,d) Primary beam size approximately 10 times larger then the grain size.

This limits the application of Laue diffraction in Material Science to simple orientation analysis and to structural investigations[6] of single crystals. Real materials are –

[4] Using the elastic constants of the material allows for the calculation of the stress tensor, as for instance done in [82]

[5] Energy is ranging from approximately 5-25keV, $2\theta_{center} = 90^{\circ}$ [48, 81]

[6] mostly used in Geology

in most cases – polycrystalline, which led to a diminishing demand of Laue diffraction during the last three decades. However, the ongoing trend to produce smaller and smaller X-ray beams at synchrotron sources allows one to study single grain properties of polycrystalline materials, leading to a renaissance of Laue diffraction: So called μLaue diffraction.

Using Laue Diffraction at the Micron Scale

μLaue offers several benefits at the micron scale in comparison to monochromatic diffraction. These advantages are based on the fact that Laue diffraction does not require any sample rotation as necessary in case of monochromatic experiments. The center of rotation should – in the monochromatic case – always coincide with the region of interest (Fig. 4.4), which is very hard to control at the micron scale. Otherwise the primary synchrotron beam moves on the sample. Furthermore, due to the non-zero depth of information, it is impossible to stay at a constant illuminated volume. Hence, rotating the sample always leads to a different illuminated volume, which hinders a quantitative analysis, except for the case that the entire grain is smaller than the primary beam size. This disadvantage does not occur with Laue diffraction.

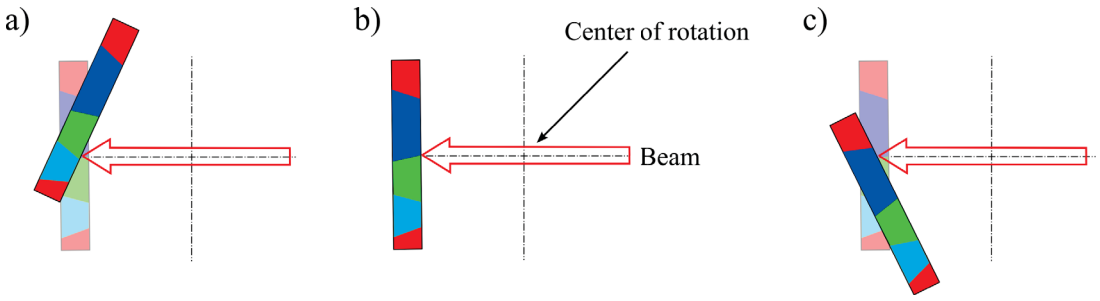

Figure 4.4: The footprint of the primary beam moves on the sample if the rotation axis does not coincide with the region of interest.

Laue diffraction is routinely used to analyze the orientation of single grains [84, 85] and measuring the strains in thin metallic films [82, 86]. Using a differential scanning aperture [87, 88] can further provide three-dimensional strain and orientation distributions with micrometer resolution [89]. This differential scanning method allows for a depth resolved analyzes of the dislocation density and type, as shown for shock deformed samples [90] or in the vicinity of interfaces [91–93].

4.2 μLaue: The Impact of Dislocations on the Laue Pattern

It is known that dislocations cause changes in the diffraction peak shape [94]. In contrast to powder diffraction, where this influence mainly stems from micro-strains, Laue diffraction is also sensitive to crystal rotations, which is mainly caused by the storage of GNDs. In this section, the influence of both, SSDs and GNDs will be discussed. Fig. 4.5 shows two different Laue patterns, (a) containing only SSDs and (b) containing both, SSDs and GNDs.

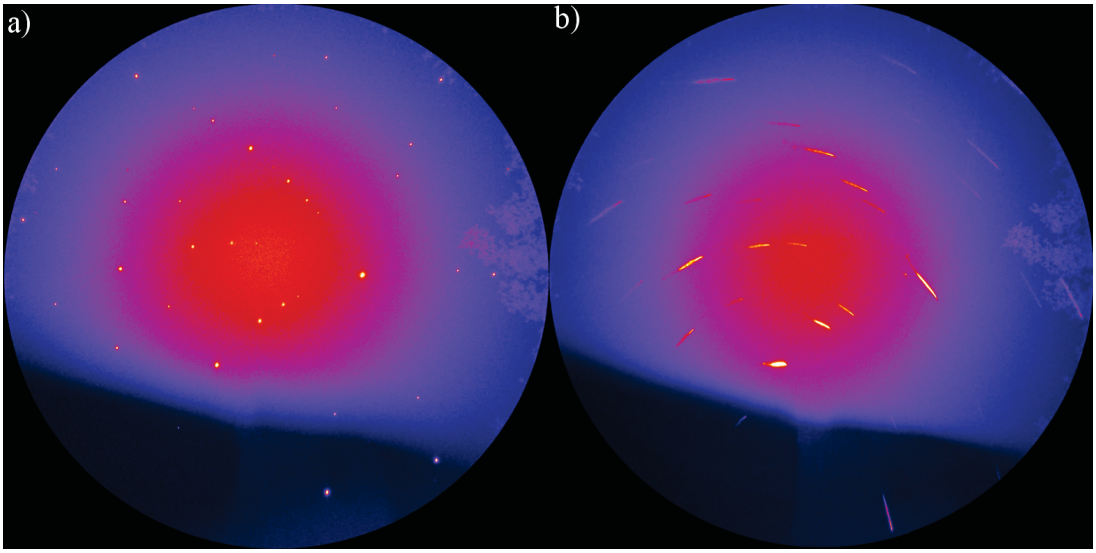

Figure 4.5: (a) Laue pattern of a crystal containing only SSDs and (b) containing both, SSDs and GNDs.

Geometrically Necessary Dislocations (GNDs)

Geometrically necessary dislocations[7] are characterized by a nonzero net-Burgers vector over a large Burgers circuit. This leads to long range strain fields, which are responsible for a lattice curvature, such as shown in Fig. 4.6. The lattice curvature can be interlinked directly to the dislocation density tensor[8], as shown by Pantleon [95] (Eq. 4.1):

$$\kappa_{ki} = \rho_{ik} - \frac{1}{2}\delta_{ki}\rho_{mm} \tag{4.1}$$

where κ is the curvature tensor, ρ is the dislocation density tensor and δ is the Kronecker-Delta. Since the illuminated volume is of finite size, the diffracting volume exhibits an orientation gradient leading to an elongated Laue spot[9]. In Fig. 4.7 a typical Laue spot shape of a GND-free crystal (a), a crystal containing one type of GNDs (b) and containing a dislocation wall consisting of one type of dislocations (c) is shown. Note that for Laue diffraction experiments, where a broad energy band pass is used, Braggs law is fulfilled for a lattice plane independent of the plane orientation and though the entire orientation spread will be projected to the detector.

The elliptical Laue spot exhibits two axes: The natural streak axis ξ and the direction ν perpendicular to it [96]. ξ can be calculated using the Eq. 4.2:

$$\underline{\xi} = \frac{\underline{u} \times \underline{G_{hkl}}}{|\underline{u} \times \underline{G_{hkl}}|} \tag{4.2}$$

[7] At the micron scale better called excess or unpaired dislocations
[8] The elastic strain tensor is neglected in this case
[9] A rudimental comparison is the reflection of a circular beam on a bent mirror, which also leads to an elliptical image of the beam.

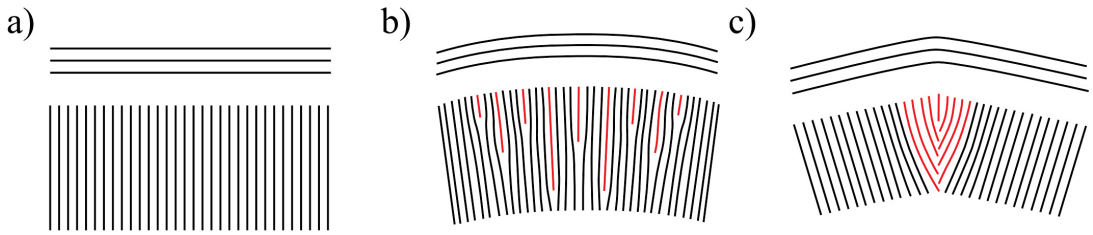

Figure 4.6: (a) Perfect, dislocation free crystal; (b) Crystal containing randomly distributed GNDs on one slip system; (c) Crystal where GNDs form a sub-grain boundary. Red lines indicate inserted half-planes which are responsible for forming the dislocation.

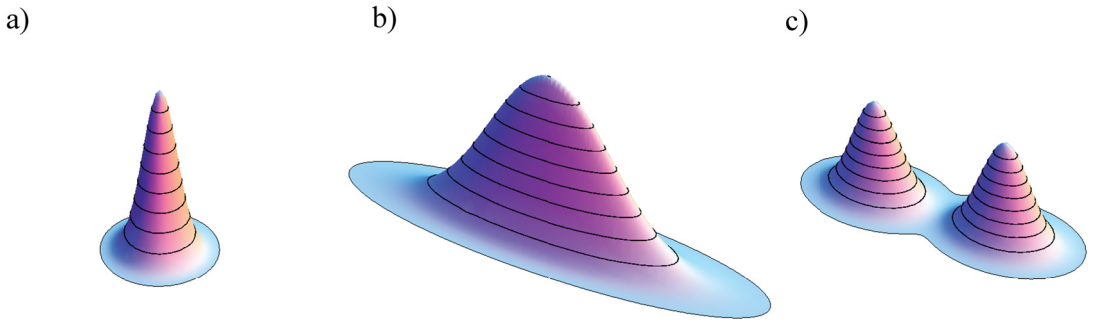

Figure 4.7: Laue spot of a (a) perfect, GND-free crystal; (b) of a crystal containing randomly distributed GNDs on one slip system; (c) of a crystal, where GNDs form a sub-grain boundary.

The direction of the measured streaks can be used to analyze the type of stored GNDs [96]. If pronounced streaking occurs, i.e. if the peak width in streaking direction is large compared to the width perpendicular to it ($\sigma_\xi \gg \sigma_\nu$), the density of GNDs can be calculated according to Eq. 4.3 [96],

$$FWHM_\xi = \rho^{GND}\, b_p\, |\underline{G_{hkl}}|\, L \sqrt{\left(1 - u\, \frac{\underline{G_{hkl}}}{|\underline{G_{hkl}}|}\right)^2} \tag{4.3}$$

with $FWHM_\xi$ being the measured *Full Width at Half Maximum (FWHM)* of the peak in direction ξ, ρ^{GND} being the density of GNDs, b_p being the projection of the Burgers vector on the primary beam path, G_{hkl} being the diffraction vector and L the length of the primary beam path.

Statistical Stored Dislocations

If – in contrast to the above described case – the peak exhibits a symmetric shape, the number of GNDs can be neglected. However, in both cases, the total stored dislocation density is proportional to the peak width in the direction ν according to Eq. 4.4.

$$FWHM_\nu = \frac{|\underline{b}|\, |\underline{G_{hkl}}|}{8(1-\nu)} \sqrt{\frac{\rho\, l}{\pi}} \tag{4.4}$$

with $|b|$ being the magnitude of the Burgers vector, ρ being the total stored dislocation density and l being a constant in the order of unity. If no peak streaking occurs, $FWHM_\nu$ is proportional to the SSD density [96].

Dislocation Boundaries

Due to the Peach-Koehler-Force (see Eq. 2.1) dislocations form patterns, resulting in regions with high dislocation density and regions with low dislocation density. According to Ice and Barabash [96] GNDs can be organized either individually, as incidental dislocation boundaries, as geometrically necessary boundaries or even in lamellar bands. However, it should be noted that such boundaries can be detected by split intensities. Probably the easiest dislocation boundary is a sub-grain boundary as shown in Fig. 4.6c resulting in two well separated Laue spots as shown in Fig. 4.7c. In fact, to observe two separated maxima the misorientation θ between two different cell blocks needs to exceed a critical angle. This angle depends not only on the instrumental resolution, but also on the averaged peak width of the cell blocks (cb). A criterion for split intensities is given in [96]:

$$K = \frac{\theta}{FWHM_{cb}} \tag{4.5}$$

According to Ice and Barabash: "*If $K < 1$, the intensity distribution of white beam reflection is continous. If $K > 1$ the white beam reflection is discontinous and the intensity profile along the streak consists of discrete spikes.*" [96]

A Critical Discussion on Experimental Limitations

Besides GNDs elastic strains can also contribute to the lattice curvature, which can be neglected in most cases. The elastically caused lattice curvature $\ddot{y}$ is proportional to the momentum M, which scales according to Eq.4.6, Eq.4.7 and Eq.4.8 reciprocally with the height h of the sample (E being the Elastic Modulus, I is being the Area Moment of Inertia, W being Elastic Section Modulus and b_b being the width of the bending beam):

$$\ddot{y} = -\frac{M_B}{EI} \tag{4.6}$$

$$\sigma = \frac{M_B}{W} = \frac{M_B}{I}e = \frac{6M_B}{b_b h^2} \tag{4.7}$$

$$\ddot{y} = -\frac{\sigma}{E}\frac{2}{h} \tag{4.8}$$

Thus, the contribution of the elastic curvature to the entire curvature increases with decreasing sample sizes and increases with the ratio σ/E. In contrast, the peak width caused by GNDs is linearly proportional to the density of GNDs (see Eq. 4.3), which is independent of the sample size.

The plot presented in Fig. 4.8 estimates the influence of elastically caused lattice curvature with assumptions given below:

- only one type of GNDs is assumed: b equals the sample x axis; u is parallel to y
- a momentum is applied at both ends of the bending beam (= sample), leading to a lattice curvature purely caused by elastic strains
- the primary beam size is $1\mu m$ in each case
- the instrumental broadening was measured at BM32 [80] of the ESRF synchrotron source using a Ge-wafer

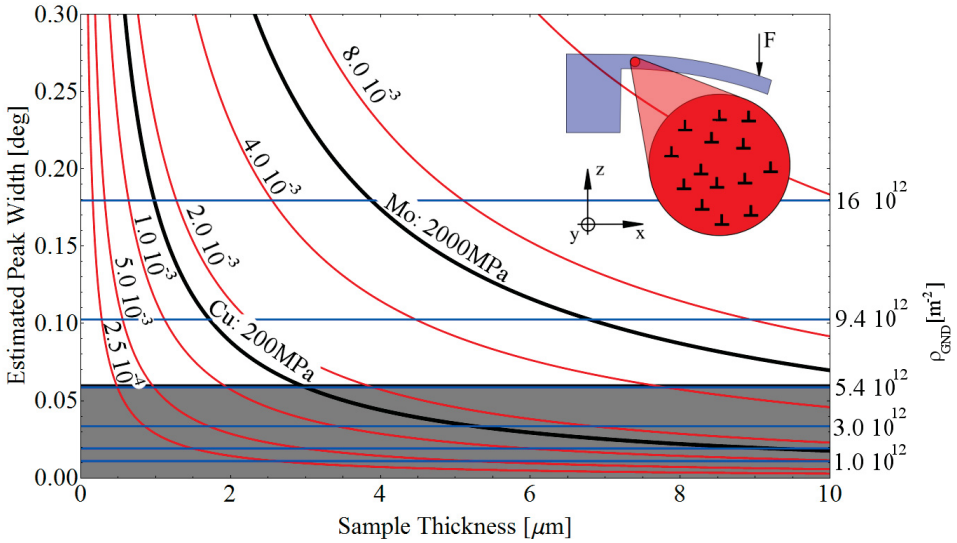

Figure 4.8: Contribution of elastic curvature tensor (red) and GNDs (blue) to the diffraction peak width. Red curves are calculated for different ratios of σ/E with the ratio given next to the line. In addition, the black curves are calculated for Cu ($200MPa$ stress) and Mo ($2000MPa$ stress), which are typical values obtainable in micro-compression experiments. Blue lines represent different GND densities given on the right side in m^{-2}. A peak width below the resolution limit (measured on a Ge-wafer) can not be measured (gray area).

The plot can be used to estimate the influence of the elastic curvature at different stress levels. For instance, copper micro samples with a diameter of $3\mu m$ typically exhibit – depending on the orientation – a flow stress of $100MPa$-$200MPa$ (see the lower black curve in Fig. 4.8). Since the stress in the sample is always lower than the yield stress, the elastically caused curvature needs to be smaller than described by the black line. Since the instrumental resolution (0.06°) is higher than the maximum elastically caused curvature of a $3\mu m$ thick sample, the elastic curvature can always be neglected in these dimensions. In contrast in Molybdenum – which is able to sustain much more stress [40] – the critical diameter where an elastic curvature can be neglected is much higher.

4.3 μLaue Diffraction and the Size Effect

R. Maaß et al. [69] presented the first μLaue experiments in the year 2006, focusing on the defect structure in micron sized compression samples. With their studies, they

impressively proved that Laue diffraction can contribute to the understanding of size dependent plasticity. The main findings are the presence of peak streaking in FIB-milled compared to *Deep Reactive Ion Etched (DRIE)* Si pillars with a diameter of $2.7\mu m$ and $1\mu m$ respectively and the fact that the investigated Au and Al pillars are far from being perfect single-crystals.

The next milestone in the understanding of size dependent plasticity was the implementation of an *in situ* μLaue testing equipment at the *Swiss Light Source (SLS)* [97], which allows for interlinking the defect structure with the stress strain response. It has been found, that the Ni micro-pillars with a diameter of $10\mu m$ containing a small-angle grain boundary exhibiting according to R. Maaß et al. *"... a strength higher or within the upper bounds of previously published values"* [46].

Further *in situ* experiments by Maaß et al. [97] showed – for the first time – a couple of deformation features, which can not only be related to the FIB-milling of the samples. All five observed Laue spots[10] indicate strain gradients (peak streaking) in a $2\mu m$ sized FIB-milled Au pillar. This continuous streaking increases during straining, but: *"During the first strain burst the peak sharpens and a satellite peak is formed,..."* [97]. The origin of the initial strain gradient is questionable and still under debate. However, the increase of peak width during straining with an abrupt formation of a sub-grain is the major finding of this study. A $10\mu m$ thick pillar shows less pronounced streaking in the initial state, but nevertheless also the formation of a satellite peak at relatively low strains and stresses.

Due to the findings in [46] additional studies, summarized in the publication *"On the initial microstructure of metallic micropillars"* [45], were performed. Micro-structural features, such as strain gradients, sub-grain boundaries and twins were found in virgin pillars, especially in pillars of small dimensions. The authors concluded that these features are partly responsible for the huge scatter in the observed yield stress values.

A.S. Budiman et al. [70] showed that the diffraction peak width of a $580nm$ sized Au pillar did not significantly increase during deforming to 0.35 strain. Furthermore, Budiman et al. found no evidence of lattice rotations and concluded: *"... plasticity here is not controlled by strain gradients, but rather by dislocation source starvation, ..."* [70]. This is in contradiction to the observations of Maaß et al. [46, 97].

Recently, Maaß et al. suggested a Laue diffraction based criterion for the definition of yield, the *Laue yield* [55] . The definition is based on observations made during their numerous experiments: Each Laue spot continuously moves in any direction during the first part of loading, but abruptly changes the moving-path and, then, follows the predicted direction. The stress measured at the point where the Laue spot changes its moving direction is called Laue yield. This is somehow expected: The position of each Laue spot depends on the deviatoric strains (shape of the unit cell) and the orientation of the crystal. The peak movement during the first loading part might be addressed to deviatoric strains. The instrumental constraints during the test can then lead to a sample rotation, which would be responsible for changes in peak movement.

[10] Due to using Laue in transmission geometry, the number of observable Laue spots is very low for experiments by Maaß and co-workers [97].

Table 4.1: μ Laue experiments contributing to the understanding of size dependent plasticity

	Material	Main Findings	Mode
R. Maaß et al. [69]	Si, Au, Al	FIB-damage present; Initially not perfectly single crystalline	*ex situ*
R. Maaß et al. [46]	Ni	Increase of yield stress due to a low-angle grain boundary	*ex* and *in situ*
R. Maaß et al. [97]	Au $[4\bar{6}3]$	Slip on unpredicted slip system for small pillar-diameters and on a predicted system for larger diameters	*in situ*
R. Maaß et al. [98]	Cu $\approx$ [001]	Stress is inhomogeneous along the sample height; Comparison of μLaue and *Electron Backscatter Diffraction (EBSD)*	*in situ*
R. Maaß et al. [45]	Au, Cu, Ni, Ni-Ti, sputtered Au	Micro-structural features: strain gradients, sub-grains, twins	*ex situ*
A.S. Budiman et al. [70]	Au	No peak broadening; Experiments fit to dislocation starvation model	*ex situ*
R. Maaß et al. [55]	Au	Substructures form well below 0.05 strain	*in situ*
R. Maaß et al. [99]	Au	Definition of the Laue yield; Strain hardening	*in situ*
C. Kirchlechner et al. [48]	Cu $\langle 234 \rangle$	Early activation of unpredicted slip system; Schematic slip mechanism maps	*ex situ*
J. Zimmermann et al. [59]	Mo-whiskers	Peak broadening due to FIB-milling	*ex situ*
C. Kirchlechner et al. [78]	Cu $\langle 234 \rangle$	Instrumental setup; Misaligned sample	*in situ*
C. Kirchlechner et al. [49]	Cu $\langle 234 \rangle$	Impact of instrumental constraints and misalignment on the peak shape	*in situ*
C. Kirchlechner et al. [100]	Cu $\langle 234 \rangle$	μLaue tensile test; Dislocation structure gets into a steady state	*in situ*

The peak movements during the elastic part should be minor and should, according to Hooke's law increase linearly with the applied stress. However, this did not occur. Furthermore, the experiments performed on single slip oriented Cu (C. Kirchlechner unpublished results and [49]) show that the Laue yield is a measure for the perfection of a compression experiment.

To summarize, μLaue experiments show that samples at the micron scale, which were expected to be single crystalline, showed features like strain gradients, sub-grains and twins [45], all known to change the strength of a material. The continuous increase of the strain gradients (streaks) typically leads to the formation of a satellite peak [97], evidencing the formation of a sub-grain. This is in contradiction to other experiments [70], which did not reveal significant changes of the diffraction peak shape. Studies focusing on size effects of plasticity are summarized in Tab. 4.1.

5 Summary of Appended Papers

The flow stress of micron sized single crystalline samples depends on the sample size, which is not reflected in classical theories. Prominent models explaining this phenomenon, i.e. dislocation starvation and dislocation source truncation, have not been validated yet. This is mainly due to the fact that instrumental constraints and experimental imperfections obscure the mechanical response of single crystalline micropillars. For a thorough understanding it is necessary to link the stress-strain response to the initial and evolving micro-structure, which requires appropriate *in situ* methods. The aim of this thesis is to provide a new insight into size dependent plasticity processes by combining two novel methods, namely constraint free micro-tensile experiments with *in situ* μLaue diffraction. In the following short summary the experimental work performed during this thesis is presented.

5.1 Dislocation storage in single slip oriented Cu micro-tensile samples: New insights by X-ray microdiffraction

Main focus of this work[1] is on the type of stored GNDs in micron sized tensile samples which were produced using the FIB workstation Zeiss 1525XB similar to Kiener et al. [30]. The samples were oriented for single slip with a nominal straining axis parallel to the [2 3 4] crystal axis. The tensile tests have been performed in the new *in situ* SEM Zeiss 982[2] using the ASMEC UNAT micro-indenter. Sample A was strained up to 0.04 engineering strain, sample B and C up to 0.25 engineering strain.

The μLaue diffraction experiments have been carried out at the French beamline CRG-IF [80] at the exit of the BM32 bending magnet synchrotron source. Hereby, the

[1] Philosophical Magazine **91** (7): 1256-1264 (2011)

[2] The SEM was modified by mounting an additional vacuum chamber.

samples were *post mortem* raster scanned with a step size of $1\mu m$.

The findings of this study are:

- The observed stress strain behavior in $3\mu m$ sized tensile samples is reproducible with a constant yield stress up to 0.18 strain, where hardening sets in.
- The hardening rates at strains higher than 0.18 are identical for sample B and C[3].
- The sample strained for 0.04 engineering strain showed peak streaking corresponding to a lower ranked slip system in the sample center, and no peak streaking in the vicinity of the sample base and head.
- The samples strained to 0.25 strain showed the storage of GNDs on the primary slip system in the vicinity of the sample base and head and a more complicated peak shape in the sample center, which is characterized by the formation of sub-grains and by the activation of more than just the primary slip system.
- The sample rotations are in agreement with Schmid's predictions for single slip.
- Based on these observations a schematic slip mechanism map can be drawn.

It can, therefore, be concluded, that at low strains a lower ranked (classically unpredicted) slip system is activated. This might well be possible since not only the Schmid factor, but also the product given by the Schmid factor times the dislocation source lengths determines the activated system. Furthermore, the complicated dislocation structures in the sample center at higher strains are a direct micro-structural evidence for the observed hardening. However, *in situ* μLaue diffraction is required to observe and quantify the evolving dislocation structure.

5.2 In situ μLaue: Instrumental setup for the deformation of micron sized samples

The need for *in situ* μLaue experiments requires an appropriate straining device for BM32. In this work[4] we present a novel, customer designed straining device which fulfills several requirements. These are:

- The device has to fit to the instrumental stage of the beamline [80].
- The primary and secondary beam must not be obstructed.
- Sample and counter-body must be independently aligned with one optical microscope.
- Vibrations coming from the ground have to be damped.
- Force and displacement have to be recorded simultaneously.

[3] Sample A was strained to only 0.04 engineering strain.

[4] Advanced Engineering Materials **doi: 10.1002\adem.201000286**

The device works in displacement controlled loop mode. Force is measured using the eigenfrequency of a $30\mu m$ thick tungsten wire with a resolution of approximately $10\mu N$. Displacement is measured and controlled at the fixed body joint of the Piezo Pu-38 (piezosystems Jena) and allows for positioning in the nm range. Fluorescence scans, μLaue image (raster) scans and *in situ* deformation are presented in the manuscript.

Furthermore, concepts for analyzing the diffraction data and an example of a compression pillar (single slip oriented, $7 \times 7 \times 21\mu m^3$) is presented showing the formation of huge streaks and sub-grains due to misalignment. Finally, the impact of the "tail" of the the primary synchrotron beam on the applicability of μLaue diffraction in submicron dimensions is discussed.

5.3 Impact of Instrumental Constraints and Imperfections on the Dislocation Structure in micron sized Cu Compression Pillars

Several studies (e.g. [1,26,27]) reported the increase of the yield stress during uniaxial compression experiments with decreasing sample size, whereas the power law exponent m as introduced in Eq. 3.4 differs from tensile experiments. This might be caused by instrumental constraints, as already discussed in [66].

In this study[5] the impact of instrumental constraints and imperfections – mainly misalignment – has been analyzed using *in situ* μLaue diffraction. Three initially identical compression pillars with a size of $7 \times 7 \times 21\mu m^3$ have been tested at BM32 of the ESRF synchrotron source, using the previously described straining device [78]. During straining the primary beam has been placed in the sample center. The μLaue experiments are complemented with *post mortem* SEM analysis. The main findings are:

- In the misaligned sample streaking is already observed at low strains, which then further increases. Streaking was, most likely, caused by edge-type GNDs on the slip system with the fifth highest Schmid factor. These dislocations are stored at low strains to accommodate the inclination between flat punch indenter and pillar top surface, and further hinder dislocation movement on the primary slip system. This leads to a polygonization of the lattice curvature forming several subgrains, evidenced by streak splitting into satellite peaks.

- In the case of an ideally aligned compression sample no excess dislocations are stored at low strains. This observation holds true for a region close to the sample center and for engineering strains lower than 0.18.

- In all cases GNDs are stored in the vicinity of the sample top surface and the sample bottom. These GNDs cannot penetrate through these surfaces and are evidence of a geometrical constraint. Furthermore, these dislocations confine the

[5] Acta Materialia **submitted manuscript** (2011)

volume which is able to freely glide and results in additional hardening (solely caused by the sample geometry).

Additional evidence for the constraint deformation has been found in the stress strain curve: The stress necessary to re-initiate plastic deformation after unloading is lower than before unloading. This behavior is caused by the lateral stiff testing equipment. This causes the formation of a lateral force which increases with ongoing plastic deformation, but vanishes when an unloading cycle is included [49].

In summary, instrumental constraints and imperfections in micron sized compression samples hinder dislocation movement and affect the stress strain response of a material, especially the hardening behavior. It is therefore questionable if micro-compression experiments on single crystalline pillars are a suitable tool to explore plasticity in small dimensions.

5.4 Expected and Unexpected Plastic Behavior at the Micron Scale: An in situ μLaue Tensile Study

In macroscopic dimensions compression tests are avoided, since undefined boundary conditions (e.g. friction, limited aspect ratio[6]) obscure the stress-strain behavior. The impact of the test conditions can – at least for the better part – be avoided when uniaxial tensile experiments are performed. In this study[7] instrumental constraints were excluded by performing tensile tests in order to unravel processes during the plastic deformation in confined volumes.

The samples have been produced using a hammer-like sample shape allowing for an accurate alignment in an optical microscope. During straining the primary X-ray beam has been placed in the sample center and load, displacement and diffraction images have been recorded simultaneously using the previously described straining device [78]. Furthermore, the samples have been raster-scanned before and after deformation.

Three different behaviors have been observed:

- Misaligned behavior: A high certainty exists that a sample is misaligned. This leads to a disastrous misinterpretation of the underlying plasticity, but fortunately can be quantified with μLaue diffraction techniques [49].

- Expected, bulk like behavior: The sample deforms on the primary slip system. No slip steps or peak streaking of an secondary slip system has been observed. The diffraction peak shape in the sample center is circular.

- Unexpected behavior: A secondary slip system is activated and stores GNDs at low strains. The streaking – and therefore the GND density – increases during straining, but is instantly reduced in a first load drop. During subsequent deformation the peak streaking reduces and the GND density in the sample center is

[6] Otherwise buckling occurs.
[7] **in preparation**

reducing due to the escape of GNDs at the sample surface. The sample center is ending up with approximately the same peak width as in the initial state.

In the case of the unexpected and the expected behavior the orientation changes of the sample center predominately follow the predictions of Schmid [101]. However, a slight deviation of this ideal rotations can be seen indicating the activation of a secondary slip system well before the geometrical predictions (see Fig. 2.7).

Both – the expected and the unexpected behavior – are ending up with a nearly GND free sample center. In the vicinity of the sample head and base edge-type GNDs are stored.[8] These dislocations are responsible for the observed rotation of the sample center and are evidence of the laterally stiff testing equipment. However, since the sample aspect ratio is 1:5 the influence of this border region to the stress-strain behavior can be neglected. The assumption that instrumental constraints do not significantly influence the material behavior is valid.

Finally, the observations in this study document that each yield criterion at low strains probes the initial dislocation structure. The yield point varies from the Peierls stress to the theoretical stress at low strains. Since a steady state GND density is reached it can be concluded that a steady state dislocation structure might be reached in the observed stress plateau and then a technical yield criterion defined in the regime of the stress-plateau is valid and feasible at the micron scale.

[8] *Post mortem* TEM analysis of this region proofed the described μLaue observations. The TEM analysis have been performed by P.J. Imrich in [102].

6
Conclusion

The yield point of single crystalline, micron sized samples is size dependent, but the validation of the two most promising models – namely dislocation source size truncation [42] and dislocation starvation [29, 44] – is hindered by imperfections and instrumental constraints during compression tests. This was proven using a novel *in situ* μLaue testing equipment established at the French beamline CRG-IF at the BM32 bending magnet synchrotron source of the European Synchrotron Radiation Facility (ESRF). Even though μLaue diffraction allows for excluding misaligned (imperfect) samples it is impossible to avoid the applied constraints during compression tests.

To avoid any instrumental constraints tensile tests have to be performed. If so, two inherently material dependent behaviors have been observed: (i) Expected, bulk like behavior where slip takes place on the primary slip system and no GNDs are stored at all. (ii) Unexpected behavior, where an unpredicted slip system is activated at low strains and stores GNDs. These GNDs pile-up, most likely at a native oxide layer or a FIB-damaged surface zone, but break through the layer and escape at the sample surface when a sufficiently high stress is applied. In both cases a stress plateau – which does not depend on the behavior but only on the size of the specimen – is formed. A technical yield criterion defined at these strains is valid and feasible at the micron scale and most likely probes a steady state dislocation structure.

7
List of Publications

7.1 Main Author Papers

Paper A
C. Kirchlechner, D. Kiener, C. Motz, S. Labat, N. Vaxelaire, O. Perroud, J.S. Micha, O.Ulrich, O. Thomas and G. Dehm, J. Keckes
Dislocation storage in single slip oriented Cu micro-tensile samples: New insights by X-ray microdiffraction
Philosophical Magazine **91** (7): 1256-1264 (2011)

Paper B
C. Kirchlechner, J. Keckes, J.S. Micha and G. Dehm
In situ μLaue: Instrumental setup for the deformation of micron sized samples
Advanced Engineering Materials **doi: 10.1002\adem.201000286**

Paper C
C. Kirchlechner, J. Keckes, W. Grosinger, M.W. Kapp, C. Motz, J.S. Micha, O. Ulrich and G. Dehm
Impact of instrumental constraints and imperfections on the dislocation structure of single crystalline Copper samples
Acta Materialia **submitted manuscript** (2011)

Paper D
C. Kirchlechner, P.J. Imrich, W. Grosinger, C. Motz, M.W. Kapp, J. Keckes, S. Labat, O. Thomas, J.S. Micha, O. Ulrich and G. Dehm
Expected and unexpected behavior at the micron scale: A μLaue study
in preparation

Paper E
C. Kirchlechner, K.J. Martinschitz, R. Daniel, C. Mitterer, J. Donges, A. Rothkirch, M. Klaus, C. Genzel and J. Keckes
X-ray diffraction analysis of three-dimensional residual stress fields reveals origins of thermal fatigue in uncoated and coated steel
Scripta Materialia **62** (10): 774-777 (2010)

Paper F
C. Kirchlechner, K.J. Martinschitz, R. Daniel, M. Klaus, C. Genzel, C. Mitterer and J. Keckes
Residual stresses and thermal fatigue in CrN hard coatings characterized by high-temperature synchrotron X-ray diffraction
Thin Solid Films **518** (8): 2090-2096 (2010)

Paper G
C. Kirchlechner, K.J. Martinschitz, R. Daniel, C. Mitterer and J. Keckes
Residual stresses in thermally cycled CrN coatings on steel
Thin Solid Films **517** (3): 1167-1171 (2008)

7.2 Co-Author Papers

Paper H
M. Rester, F.D. Fischer, C. Kirchlechner, T. Schmoelzer, H. Clemens and G. Dehm
Deformation mechanisms in micron-sized PST TiAl compression samples: Experiment and model
Acta Materialia **59** (9): 3410-3421 (2011)

Paper I
N. Vaxelaire, S. Labat, V. Chamard, O. Thomas, V. Jacques, F. Picca, S. Ravy, C. Kirchlechner and J. Keckes
3D strain imaging in sub-micrometer crystals using cross-reciprocal space measurements: Numerical feasibility and experimental methodology
Nuclear Instruments and Methods in Physics Research Section B: Beam Interactions with Materials and Atoms **268** (3-4): 388-393 (2010)

Paper J
N. Vaxelaire, H. Proudhon, S. Labat, C. Kirchlechner, J. Keckes, V. Jacques, S. Ravy, S. Forest and O. Thomas
Methodology for studying strain inhomogeneities in polycrystalline thin films during in situ thermal loading using coherent X-ray diffraction
New Journal of Physics **12** (3): (2010)

Paper K

K.J. Martinschitz, C. Kirchlechner, R. Daniel, G. Maier, C. Mitterer, J. Keckes
Temperature dependence of residual stress gradients in shot-peened steel coated with CrN
Materials Science Forum, **571-572**: 101-106 (2008)

References

[1] M. D. Uchic, D. M. Dimiduk, J. N. Florando, and W. D. Nix. Sample dimensions influence strength and crystal plasticity. Science, 305(5686):986–989, 2004.

[2] G. Gottstein. Physikalische Grundlagen der Materialkunde, chapter Mechanische Eigenschaften, pages 197–207. Springer, 2001.

[3] H. Blumenauer. Werkstoffprüfung, chapter Werkstoffmechanische Prüfung, page 105. Deutscher Verlag für Grundstoffindustrie, 1994.

[4] J. Weertmann and J. R. Weertmann. Elementary Dislocation Theory, chapter Description of a Dislocation, pages 15–16. Oxford University Press, 1992.

[5] G. Gottstein. Physikalische Grundlagen der Materialkunde, chapter Kristallbaufehler, pages 65–67. Springer, 2001.

[6] D. Hull and D.J. Bacon. Introduction to Dislocations, chapter Defects in Crystals, pages 17–20. Butterworth-Heinemann, 2001.

[7] D. Hull and D.J. Bacon. Introduction to Dislocations, chapter Elastic Properties of Dislocations, pages 69–72. Butterworth-Heinemann, 2001.

[8] G. Gottstein. Physikalische Grundlagen der Materialkunde, chapter Mechanische Eigenschaften, page 221. Springer, 2001.

[9] J. Weertmann and J. R. Weertmann. Elementary Dislocation Theory, chapter Forces on a Dislocation, pages 45–52. Oxford University Press, 1992.

[10] E. Schmid and W. Boas. Kristallplastizität. Zeitschrift fr Elektrochemie und angewandte physikalische Chemie, 41:638, 1935.

[11] H.P. Stüwe. Einführung in die Werkstoffkunde, chapter Plastische Verformung, page 106. B.I. Wissenschaftsverlag, 1978.

[12] G. Gottstein. Physikalische Grundlagen der Materialkunde, chapter Der atomistische Aufbau der Festkörper, pages 36–41. Springer, 2001.

[13] F. C. Frank and W. T. Read. Multiplication processes for slow moving dislocations. Phys. Rev., 79(4):722–723, 1950.

[14] W. D. Nix and S.W. Lee. Micro-pillar plasticity controlled by dislocation nucleation at surfaces. Philosophical Magazine, 91(7):1084–1096, 2011.

[15] J. Weertmann and J. R. Weertmann. Elementary Dislocation Theory, chapter Dislocation Multiplication, pages 123–126. Oxford University Press, 1992.

[16] S.W. Lee and W.D. Nix. Geometrical analysis of 3D dislocation dynamics simulations of fcc micro-pillar plasticity. Materials Science and Engineering: A, 527(7-8):1903 – 1910, 2010.

[17] J. Weertmann and J. R. Weertmann. Elementary Dislocation Theory, chapter Image Forces, pages 168–173. Oxford University Press, 1992.

[18] E. O. Hall. The deformation and ageing of mild steel .3. discussion of results. Proceedings of the Physical Society of London Section B, 64(381):747–753, 1951.

[19] N. J. Petch. The cleavage strength of polycrystals. Journal of the Iron and Steel Institute, 174(1):25–28, 1953.

[20] E. Arzt. Size effects in materials due to microstructural and dimensional constraints: A comparative review. Acta Materialia, 46(16):5611 – 5626, 1998.

[21] N.A. Fleck, G.M. Muller, M.F. Ashby, and J.W. Hutchinson. Strain gradient plasticity: Theory and experiment. Acta Metallurgica et Materialia, 42(2):475 – 487, 1994.

[22] J. S. Stölken and A. G. Evans. A microbend test method for measuring the plasticity length scale. Acta Materialia, 46(14):5109 – 5115, 1998.

[23] J. G. Swadener, E. P. George, and G. M. Pharr. The correlation of the indentation size effect measured with indenters of various shapes. Journal of the Mechanics and Physics of Solids, 50(4):681 – 694, 2002.

[24] W.D. Nix and H. Gao. Indentation size effects in crystalline materials: A law for strain gradient plasticity. Journal of the Mechanics and Physics of Solids, 46(3):411 – 425, 1998.

[25] D.M. Dimiduk, M.D. Uchic, and T.A. Parthasarathy. Size-affected single-slip behavior of pure nickel microcrystals. Acta Materialia, 53(15):4065 – 4077, 2005.

[26] C. A. Volkert and E. T. Lilleodden. Size effects in the deformation of sub-micron Au columns. Philosophical Magazine, 86:5567–5579, 2006.

[27] J.R. Greer, W.C. Oliver, and W.D. Nix. Size dependence of mechanical properties of gold at the micron scale in the absence of strain gradients. Acta Materialia, 53(6):1821 – 1830, 2005.

[28] J.R. Greer, W.C. Oliver, and W.D. Nix. Corrigendum to size dependence in mechanical properties of gold at the micron scale in the absence of strain gradients [Acta Mater 53 (6) (2005) 1821-1830]. Acta Materialia, 54(6):1705 – 1705, 2006.

[29] J. R. Greer and W. D. Nix. Nanoscale gold pillars strengthened through dislocation starvation. Physical Review B, 73(24):245410, 2006.

[30] D. Kiener, W. Grosinger, G. Dehm, and R. Pippan. A further step towards an understanding of size-dependent crystal plasticity: In situ tension experiments of miniaturized single-crystal copper samples. Acta Materialia, 56(3):580 – 592, 2008.

[31] A.S. Schneider, C.P. Frick, B.G. Clark, P.A. Gruber, and E. Arzt. Influence of orientation on the size effect in bcc pillars with different critical temperatures. Materials Science and Engineering: A, 528(3):1540 – 1547, 2011.

[32] A.S. Schneider, B.G. Clark, C.P. Frick, P.A. Gruber, and E. Arzt. Effect of orientation and loading rate on compression behavior of small-scale Mo pillars. Materials Science and Engineering: A, 508(1-2):241 – 246, 2009.

[33] A.S. Schneider, B.G. Clark, C.P. Frick, P.A. Gruber, and E. Arzt. Corrigendum to effect of orientation and loading rate on compression behavior of small-scale mo pillars [Mater. Sci. Eng. a 508 (2009) 241-246]. Materials Science and Engineering: A, 527(4-5):1280 – 1280, 2010.

[34] J.Y. Kim, D. Jang, and J.R. Greer. Tensile and compressive behavior of tungsten, molybdenum, tantalum and niobium at the nanoscale. Acta Materialia, 58(7):2355 – 2363, 2010.

[35] J.Y. Kim and J.R. Greer. Tensile and compressive behavior of gold and molybdenum single crystals at the nano-scale. Acta Materialia, 57(17):5245 – 5253, 2009.

[36] M.D. Uchic, P.A. Shade, and D.M. Dimiduk. Plasticity of micrometer-scale single crystals in compression. Annual Review of Materials Research, 39(1):361–386, 2009.

[37] G. Dehm. Miniaturized single-crystalline fcc metals deformed in tension: New insights in size-dependent plasticity. Progress in Materials Science, 54(6):664 – 688, 2009.

[38] O. Kraft, P. A. Gruber, R. Mönig, and D. Weygand. Plasticity in confined dimensions. Annual Review of Materials Research, 40(1):293–317, 2010.

[39] S.S. Brenner. Growth and properties of whiskers. Science, 128(3324):569–575, 1958.

[40] H. Bei, S. Shim, E.P. George, M.K. Miller, E.G. Herbert, and G.M. Pharr. Compressive strengths of molybdenum alloy micro-pillars prepared using a new technique. Scripta Materialia, 57(5):397 – 400, 2007.

[41] H. Bei, S. Shim, G.M. Pharr, and E.P. George. Effects of pre-strain on the compressive stress-strain response of Mo-alloy single-crystal micropillars. Acta Materialia, 56(17):4762 – 4770, 2008.

[42] T. A. Parthasarathy, S. I. Rao, D. M. Dimiduk, M. D. Uchic, and D. R. Trinkle. Contribution to size effect of yield strength from the stochastics of dislocation source lengths in finite samples. Scripta Materialia, 56(4):313 – 316, 2007.

[43] K.S. Ng and A.H.W. Ngan. Breakdown of Schmid's law in micropillars. Scripta Materialia, 59(7):796 – 799, 2008.

[44] W. D. Nix, J. R. Greer, G. Feng, and E.T. Lilleodden. Deformation at the nanometer and micrometer length scales: Effects of strain gradients and dislocation starvation. Thin Solid Films, 515(6):3152 – 3157, 2007.

[45] R. Maaß, S. Van Petegem, J. Zimmermann, C.N. Borca, and H. Van Swygenhoven. On the initial microstructure of metallic micropillars. Scripta Materialia, 59(4):471 – 474, 2008.

[46] R. Maaß, S. Van Petegem, D. Grolimund, H. Van Swygenhoven, and M.D. Uchic. A strong micropillar containing a low angle grain boundary. Applied Physics Letters, 89, 2007.

[47] D. Kiener, C. Motz, M. Rester, M. Jenko, and G. Dehm. FIB damage of Cu and possible consequences for miniaturized mechanical tests. Materials Science and Engineering: A, 459(1-2):262 – 272, 2007.

[48] C. Kirchlechner, D. Kiener, C. Motz, S. Labat, N. Vaxelaire, O. Perroud, J. S. Micha, O. Ulrich, O. Thomas, G. Dehm, and J. Keckes. Dislocation storage in single slip-oriented Cu micro-tensile samples: new insights via x-ray microdiffraction. Philosophical Magazine, 91(7):1256–1264, 2011.

[49] C. Kirchlechner, J. Keckes, W. Grosinger, M.W. Kapp, J.S. Micha, O. Ulrich, and G. Dehm. Impact of instrumental constraints and imperfections on the dislocation structure in micron sized Cu pillars. Acta Materialia, submitted manuscript, 2011.

[50] D. Kiener, C. Motz, and G. Dehm. Micro-compression testing: A critical discussion of experimental constraints. Materials Science and Engineering: A, 505(1-2):79 – 87, 2009.

[51] J. Senger, D. Weygand, C. Motz, P. Gumbsch, and O. Kraft. Aspect ratio and stochastic effects in the plasticity of uniformly loaded micrometer-sized specimens. Acta Materialia, In Press:–, 2011.

[52] A. J. Bushby and D. J. Dunstan. Size effects in yield and plasticity under uniaxial and non-uniform loading: Experiment and theory. Philosophical Magazine, 91(7):1037–1049, 2011.

[53] D.M. Norfleet, D.M. Dimiduk, S.J. Polasik, M.D. Uchic, and M.J. Mills. Dislocation structures and their relationship to strength in deformed nickel microcrystals. Acta Materialia, 56(13):2988 – 3001, 2008.

[54] S.H. Oh, M. Legros, D. Kiener, and G. Dehm. In situ observation of dislocation nucleation and escape in a submicrometre aluminium single crystal. Nat Mater, 8(2):95–100, 2009.

[55] R. Maaß, Van Petegem S., Ma D., Zimmermann J., Grolimund D., Roters F., Van Swygenhoven H., and Raabe D. Smaller is stronger: The effect of strain hardening. Acta Materialia, 57(20):5996 – 6005, 2009.

[56] H. Tang, K. W. Schwarz, and H. D. Espinosa. Dislocation escape-related size effects in single-crystal micropillars under uniaxial compression. Acta Materialia, 55(5):1607–1616, 2007.

[57] H. Tang, K. W. Schwarz, and H. D. Espinosa. Dislocation-source shutdown and the plastic behavior of single-crystal micropillars. Physical Review Letters, 100(18):185503, 2008.

[58] C. Motz, D. Weygand, J. Senger, and P. Gumbsch. Initial dislocation structures in 3-D discrete dislocation dynamics and their influence on microscale plasticity. Acta Materialia, 57(6):1744 – 1754, 2009.

[59] J. Zimmermann, S. Van Petegem, H. Bei, D. Grolimund, E.P. George, and H. Van Swygenhoven. Effects of focused ion beam milling and pre-straining on the microstructure of directionally solidified molybdenum pillars: A laue diffraction analysis. Scripta Materialia, 62(10):746 – 749, 2010.

[60] C. Motz, T. Schöberl, and R. Pippan. Mechanical properties of micro-sized copper bending beams machined by the focused ion beam technique. Acta Materialia, 53(15):4269 – 4279, 2005.

[61] Z. W. Shan, Raja K. Mishra, S. A. Syed Asif, Oden L. Warren, and Andrew M. Minor. Mechanical annealing and source-limited deformation in submicrometre-diameter Ni crystals. Nat Mater, 7(2):115–119, February 2008.

[62] J. R. Greer and W. D. Nix. Size dependence in mechanical properties of gold at the micron scale in the absence of strain gradients. Applied Physics A-materials Science & Processing, 90(1):203–203, 2008.

[63] H. Zhang, B.E. Schuster, Q. Wei, and K.T. Ramesh. The design of accurate micro-compression experiments. Scripta Materialia, 54(2):181 – 186, 2006.

[64] Y.S. Choi, M.D. Uchic, T.A. Parthasarathy, and D.M. Dimiduk. Numerical study on microcompression tests of anisotropic single crystals. Scripta Materialia, 57(9):849 – 852, 2007.

[65] J. Senger, D. Weygand, C. Motz, P. Gumbsch, and O. Kraft. Evolution of mechanical response and dislocation microstructures in small-scale specimens under slightly different loading conditions. Philosophical Magazine, 90(5):617–628, 2010.

[66] D. Kiener, W. Grosinger, and G. Dehm. On the importance of sample compliance in uniaxial microtesting. Scripta Materialia, 60(3):148 – 151, 2009.

[67] F. Roters, P. Eisenlohr, L. Hantcherli, D.D. Tjahjanto, T.R. Bieler, and D. Raabe. Overview of constitutive laws, kinematics, homogenization and multi-scale methods in crystal plasticity finite-element modeling: Theory, experiments, applications. Acta Materialia, 58(4):1152 – 1211, 2010.

[68] D. Kiener and A.M. Minor. Source-controlled yield and hardening of cu(100) studied by in situ transmission electron microscopy. Acta Materialia, 59(4):1328 – 1337, 2011.

[69] R. Maaß, D. Grolimund, S. Van Petegem, M. Willimann, M. Jensen, H. Van Swygenhoven, T. Lehnert, M. A. M. Gijs, C. A. Volkert, E. T. Lilleodden, and R. Schwaiger. Defect structure in micropillars using x-ray microdiffraction. Applied Physics Letters, 89, 2006.

[70] A.S. Budiman, S.M. Han, J.R. Greer, N. Tamura, J.R. Patel, and W.D. Nix. A search for evidence of strain gradient hardening in au submicron pillars under uniaxial compression using synchrotron X-ray microdiffraction. Acta Materialia, 56(3):602 – 608, 2008.

[71] J. Miao, T. Ishikawa, B. Johnson, E.H. Anderson, B. Lai, and K. O. Hodgson. High resolution 3D X-ray diffraction microscopy. Phys. Rev. Lett., 89(8):088303, 2002.

[72] S. Labat, V. Chamard, and O. Thomas. Local strain in a 3d nano-crystal revealed by 2D coherent X-ray diffraction imaging. Thin Solid Films, 515(14):5557 – 5562, 2007.

[73] N. Vaxelaire, S. Labat, V. Chamard, O. Thomas, V. Jacques, F. Picca, S. Ravy, C. Kirchlechner, and J. Keckes. 3D strain imaging in sub-micrometer crystals using cross-reciprocal space measurements: Numerical feasibility and experimental methodology. Nuclear Instruments and Methods in Physics Research Section B: Beam Interactions with Materials and Atoms, 268(3-4):388 – 393, 2010.

[74] D. Hull and D.J. Bacon. Introduction to Dislocations, chapter Dislocations in Face-centered Cubic Metals, pages 82–101. Butterworth-Heinemann, 2001.

[75] W. Friedrich, P. Knipping, and M. von Laue. Interferenz-Erscheinungen bei Röntgenstrahlen. Sitzungsbericht Mathematisch Physikalische Klasse, Bayrische Akademie der Wissenschaften:302–322, 1912.

[76] P. Ewald. Zur Theorie der Interferenzen der Röntgenstrahlen in Kristallen. Phys. Z., 14:465–472, 1913.

[77] M. De Graef and M.E. McHenry. Structure of Materials, chapter Structure Factor, pages 305–307. Cambridge University Press, 2007.

[78] C. Kirchlechner, J. Keckes, J.S. Micha, and G. Dehm. *In situ* μlaue: Instrumental setup for the deformation of micron sized samples. Advanced Engineering Materials, doi: 10.1002\adem.201000286, 2011.

[79] J.S. Chung and G.E. Ice. Automated indexing for texture and strain measurement with broad-bandpass X-ray microbeams. Journal of Applied Physics, 86(9):5249–5255, 1999.

[80] O. Ulrich, X. Biquard, P. Bleuet, O. Geaymond, P. Gergaud, J. S. Micha, O. Robach, and F. Rieutord. A new white beam X-ray microdiffraction setup on the BM32 beamline at the European Synchrotron Radiation Facility. Review of Scientific Instruments, 82(3):033908, 2011.

[81] A. A. MacDowell, R. S. Celestre, N. Tamura, R. Spolenak, B. Valek, W. L. Brown, J. C. Bravman, H. A. Padmore, B. W. Batterman, and J. R. Patel. Submicron X-ray diffraction. Nuclear Instruments and Methods in Physics Research Section A: Accelerators, Spectrometers, Detectors and Associated Equipment, 467-468(Part 2):936 – 943, 2001.

[82] O. Perroud, R. Vayrette, C. Rivero, O. Thomas, J.-S. Micha, and O. Ulrich. X-ray microbeam strain investigation on Cu-mems structures. Microelectronic Engineering, 87(3):394 – 397, 2010.

[83] N. Tamura, H.A. Padmore, and J.R. Patel. High spatial resolution stress measurements using synchrotron based scanning X-ray microdiffraction with white or monochromatic beam. Materials Science and Engineering: A, 399(1-2):92 – 98, 2005. Measurement and Interpretation of Internal/Residual Stresses.

[84] K.R. Magid, R.D. Nyilas, and R. Spolenak. Metal plasticity by grain rotation–microdiffraction case studies. Materials Science and Engineering: A, 524(1-2):33 – 39, 2009.

[85] G.E. Ice and Judy W.L. Pang. Tutorial on X-ray microlaue diffraction. Materials Characterization, 60(11):1191 – 1201, 2009.

[86] N. Tamura, M. Kunz, K. Chen, R.S. Celestre, A.A. MacDowell, and T. Warwick. A superbend X-ray microdiffraction beamline at the advanced light source. Materials Science and Engineering: A, 524(1-2):28 – 32, 2009.

[87] W. Yang, B.C. Larson, J.Z. Tischler, G.E. Ice, J.D. Budai, and W. Liu. Differential-aperture X-ray structural microscopy: a submicron-resolution three-dimensional probe of local microstructure and strain. Micron, 35(6):431 – 439, 2004.

[88] W. Liu, G.E. Ice, B.C. Larson, W. Yang, and J.Z. Tischler. Nondestructive three-dimensional characterization of grain boundaries by X-ray crystal microscopy. Ultramicroscopy, 103(3):199 – 204, 2005.

[89] G.E. Ice, J.W.L. Pang, R.I. Barabash, and Y. Puzyrev. Characterization of three-dimensional crystallographic distributions using polychromatic X-ray microdiffraction. Scripta Materialia, 55(1):57 – 62, 2006.

[90] R.I. Barabash, G.E. Ice, M. Kumar, J. Ilavsky, and J. Belak. Polychromatic microdiffraction analysis of defect self-organization in shock deformed single crystals. International Journal of Plasticity, 25(11):2081 – 2093, 2009.

[91] T. Ohashi, R.I. Barabash, J.W.L. Pang, G.E. Ice, and O.M. Barabash. X-ray microdiffraction and strain gradient crystal plasticity studies of geometrically necessary dislocations near a ni bicrystal grain boundary. International Journal of Plasticity, 25(5):920 – 941, 2009.

[92] R.I. Barabash, H. Bei, Y.F. Gao, and G.E. Ice. Interface strength in NiAl-Mo composites from 3-D X-ray microdiffraction. Scripta Materialia, 64(9):900 – 903, 2011.

[93] B.C. Larson, W. Yang, J.Z. Tischler, G.E. Ice, J.D. Budai, W. Liu, and H. Weiland. Micron-resolution 3-D measurement of local orientations near a grain-boundary in plane-strained aluminum using X-ray microbeams. International Journal of Plasticity, 20(3):543 – 560, 2004.

[94] T. Ungár. Microstructural parameters from X-ray diffraction peak broadening. Scripta Materialia, 51(8):777 – 781, 2004. Viewpoint set no. 35. Metals and alloys with a structural scale from the micrometer to the atomic dimensions.

[95] W. Pantleon. Resolving the geometrically necessary dislocation content by conventional electron backscattering diffraction. Scripta Materialia, 58(11):994 – 997, 2008.

[96] G.E. Ice and R.I. Barabash. Chapter 79: White beam microdiffraction and dislocations gradients. volume 13 of Dislocations in Solids, pages 499 – 601. Elsevier, 2007.

[97] R. Maaß, S. Van Petegem, H. Van Swygenhoven, P.M. Derlet, C. A. Volkert, and D. Grolimund. Time-resolved Laue diffraction of deforming micropillars. Physical Review Letters, 99, 2007.

[98] R. Maaß, S. Van Petegem, D. Grolimund, H. Van Swygenhoven, D. Kiener, and G. Dehm. Crystal rotation in Cu single crystal micropillars: In situ Laue and electron backscatter diffraction. Applied Physics Letters, 92, 2008.

[99] R. Maaß, S. Van Petegem, C.N. Borca, and H. Van Swygenhoven. In situ Laue diffraction of metallic micropillars. Materials Science and Engineering: A, 524(1-2):40 – 45, 2009.

[100] C. Kirchlechner, Peter J. Imrich, Wolfgang Grosinger, W. Kapp, Marlene, C. Motz, J. Keckes, S. Labat, O. Thomas, J.S. Micha, O. Ulrich, and G. Dehm.

Expected an unexpected plasticity at the micron scale: A μlaue study. in preparation, 2011.

[101] H. Mark, M. Polanyi, and E. Schmid. Processes in the rotation of zinc crystals. II Announcement - quantitative determination of rotation expansion mechanism. ZEITSCHRIFT FUR PHYSIK, 12:78–110, 1923.

[102] P.J.Imrich. TEM analysis of dislocation structures in miniaturized copper tensile samples. Master's thesis, Montanuniversität Leoben, 2010.

Index

Due to copyright reasons appended papers are not included in this version of the thesis.